Liquid-Gas Phase Transition in Nuclear Matter Within Relativistic Mean Field Theory

A Dissertation

Submitted in Partial Fulfillment of the Requirement for the Award of Degree of

Master of Science

In

Physics

Submitted By:

Vishal Parmar

Roll No. 301704035

Under the supervision of:

Dr. Manoj K. Sharma
Professor
TIET Patiala

Dr. S. K. Patra
Professor
IOP Bhubaneswar

SCHOOL OF PHYSICS AND MATERIALS SCIENCE

THAPAR INSTITUTE OF ENGINEERING AND TECHNOLOGY, PATIALA

PUNJAB-147004

JUNE-2019

Dedicated to My Mother,

My Strongest Support.

Declaration

I hereby declare that the dissertation entitled **"Liquid-Gas Phase Transition in Nuclear Matter Within Relativistic Mean Field Theory"** is an authentic record of my work carried out as requirement for the the award of the degree of **Master of Science** at **Thapar Institute of Engineering and Technology, Patiala** under the supervision of **Dr. Manoj K. Sharma**, Professor, School of Physics and Materials Science, Thapar Institute of Engineering and Technology, Patiala and **Dr. S. K. Patra**, Professor, Institute of Physics Bhubaneswar. No part of the matter embodied in this dissertation has been submitted to any other university or institute for the award of any degree.

03/06/2019
Dated:

(Vishal Parmar)
301704035

It is certified that the above statement made by the student is correct to the best of my knowledge and belief.

(Dr. Manoj K. Sharma)
Supervisor
Professor
TIET, Patiala

(Dr. S. K. Patra)
Supervisor
Professor
IOP Bhubaneswar

Dr. S. K. Patra
Professor
Institute of Physics
Bhubaneswar-751005, India

Acknowledgment

I wish to acknowledge with a most heartfelt sense of gratitude for the opportunity and valuable guidance rendered on me by **Dr S. K. Patra**, Professor, Institute of Physics Bhubneshwar and **Dr Manoj K. Sharma**, Professor, Thapar Institute of Engineering and Technology. I am incredibly thankful to them for their humility to take me as their student and believing in me to undertake the problem I was given during this work. I pour my special and sincere gratitude towards **Dr S. K. Patra** for his constant support and his knowledge about the subject which is the backbone of this dissertation. I am thankful to **Dr Manoj K. Sharma** for giving me the flexibility and liberty to carry out this work.

I am also grateful to the Institute of Physics, Bhubaneshwar for the facility and resources provided during the progression of this work.

I am highly obliged to **Dr O. P. Pandey**, Head of Department, School of Physics and Materials Science and **Dr S. S. Bhatia**, Dean of academic affair for their guidance during various stage of this work. I want to embrace this opportunity to acknowledge my gratitude towards all the faculty members of the School of Physics and Materials science who were always accessible and helpful.

At last, I wish to sincerely thank all the scientists who devoted their entire life in the pursuit of truth and understanding of how nature behaves the way it does.

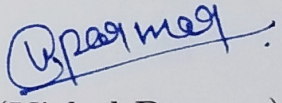

(Vishal Parmar)

Contents

List of Tables

List of Figures

Abstract

The Relativistic Mean Field Theory is used to calculate the equation of state for the symmetric and asymmetric nuclear matter at zero and finite temperature limit using the recently developed force parameters such as FSUGarnet, IOPB-I and G3 along with the widely used NL3 set. The versatility of these parameters set is investigated for a broad range of baryon density. Nuclear matter properties at zero temperature are investigated, and the results are compared with the one available in the literature. It is observed that these parameter sets are in excellent agreement with the available experimental data for both finite and infinite nuclear matter. This fact is then exploited to estimate the equation of state at finite temperature. For the first time, FSUGarnet, IOPB-I and G3 parameter sets are used here to investigate the liquid-gas phase transition in symmetric as well as asymmetric nuclear matter. The results obtained for the critical parameters are compared with the theoretical models, and recently published experimental data obtained from two compound nuclear and four multi-fragment processes. In our calculations, the critical temperature for the symmetric nuclear matter lies in the range of (13.6 - 14.3) MeV with the corresponding critical pressure P_c and critical density ρ_c in the range (0.16 - 0.19) MeV fm $^{-3}$ and (0.048 - 0.062) fm^{-3} respectively. The effect of scalar meson σ and vector meson ρ in the context of finite temperature equation of state is also investigated.

Chapter 1

Introduction and Literature Review

1.1 Introduction

About a century ago, the Rutherford gold foil scattering experiment laid the foundation of nuclear physics and was revolutionised by the discovery of the neutron by J. Chadwick in 1932. He calculated the mass of neutron by examining the scattering data of uncharged radiation produced when Beryllium was irradiated with alpha particles originating from Polonium source [1]. The discovery of neutron led to some groundbreaking development in atomic physics which gave a comprehensive picture of an atom and immediately became a new tool to probe nuclear structure. Meanwhile, in 1926, Schrödinger formulated the quantum mechanical equation based on probability theory that gave physicists an ultimate tool to handle the microscopic physics [2]. Both of these radical discoveries challenged the core philosophical foundation of science. It forced the scientific community to rethink and redevelop the fundamental aspects of nature. The time tested classical formalism had to be replaced by less intuitive probabilistic theories. After successfully understanding the behaviour of an electron in a central field produced by a huge charge centre, the next enormous challenge was to understand the nuclear phenomenon. The size is reduced considerably when one jump from the atomic to the nuclear domain and the order of energy increases from KeV to MeV. The conventional quantum mechanical formalism passed this test and accurately estimated the experimental data emanating from the deuteron problem [3]. However, this formalism failed to describe many intrinsic features of the nucleus, as the strong interaction was not well understood until then.

Though the thrust was to discover heavier nuclei, the physicists were yet to have an understanding which may explain the behaviour of strong interactions and related structural and dynamical aspects. It was not possible to use the non-relativistic Schrödinger's equation for each nucleon in these heavy nuclei in the wake of computation requirement which remains a challenge yet today. Therefore, to handle the many nucleon systems,

several phenomenological models were introduced that begin at some intermediate level, rather than solving the Schrödinger equation for each nucleon. These models were phenomenal when investigated in their respective domain such as shell model and liquid drop model. Some advance semi-classic model like the collective model was also developed, but all of these could not reproduce the entire picture of nuclear behaviour[4, 5].

Einstein parallelly in 1916, proposed yet another revolutionary idea of relativity which was confirmed by various experiments in the last century and in recent by observation of gravitational wave by LIGO and VERGO detectors [6] and the picture of Black Hole by Event Horizon Telescope [7]. It helped to explain the phenomenon like spin-orbit coupling and hyperfine structure in hydrogen [8]. Realising the essence of relativistic motion of particles, Feynman and Dyson [9] combined the classical, quantum and relativistic physics to formulate what we know as Quantum Electrodynamics (QED) and ultimately into Quantum Field Theory by several physicists, which describes the interactions in terms of the field which are more fundamental than the particles [10]. As nucleons are hadrons that are bound state of two or more quarks, the interaction between them is described well within the Quantum Chromodynamics (QCD), but instead, a more effective theory, Quantum Hadrodynamics (QHD) is used at low energy for baryons.

In this dissertation, we endeavour to understand the nuclear matter using these relativistic field theories under various parameters like density and temperature. It helps us to examine the nuclear phenomena outside the conventional nuclear physics boundaries. With the confirmation of Gravitational Wave, a new front to nuclear physics has been opened in the form of neutron stars. The behaviour and properties of the neutron star are of particular interest for both nuclear physicist and astrophysicist in order to extract the hidden knowledge about the fundamental interaction among particles.

1.2 Nuclear Matter

Weizsacker in 1935 developed the Semi-Empirical Liquid-Drop Model proposed by George Gamow which explained properties like binding energy, fission and fusion remarkably well [11]. According to this very insightful yet simplistic model, nucleons are uniformly distributed inside a nucleus and are bound by nuclear forces while the Coulomb interaction accounts for repulsion among the protons. This formula made a significant impact in

developing the semiclassical picture of the nucleus, but a more sophisticated and holistic approach was required to explain the specific nuclear properties like charge distribution, magnetic moment, cross-section etc. In principle, one should solve the Schrödinger equation for each nucleon which includes three or many body interaction potentials as expected from meson field theory proposed by Hideki Yukawa in 1986 [12]. Computing such a system of the coupled differential equation for more than two nucleons (many-body problem) is extremely time taking and complex. Therefore evaluating a nuclear system from the first principle is not feasible and instead, phenomenological models like Shell Model are frequently used which are built as per available knowledge of nuclear properties and then subsequently refined according to experimental results.

The problem becomes relatively easy if one assumes nucleons to be infinite which are distributed uniformly over infinite volume with no Coulomb interaction. Such a hypothetical system is called Infinite Nuclear Matter. If we put A (number of nucleons) $\rightarrow \infty$ in Semi-empirical formula, the surface properties become negligible compared to bulk properties. For the symmetric case, the number of neutrons is equal to the number of protons (N=Z), the symmetric energy vanishes, and only the volume term remains. This symmetric infinite nuclear matter has binding energy $\frac{E}{A} \approx -15.7$ MeV. Furthermore, considering the nuclear matter as degenerate Fermi gas, the Fermi wave number at saturation (K_F^0) is estimated to be 1.42 fm^{-1} and hence the corresponding saturation density ≈ 0.15 fm^{-3} [13].

1.3 Neutron Star

The matter at the core of heaviest known nuclei resemble the definition of nuclear matter and have the $K_F^0 = 1.36 \pm 0.06$ fm^{-1} [14]. The other possibility lies in the Neutron Star which is a remnant collapsed core of a massive star. Neutron star was theoretically predicted by Volkoff and Oppenheimer in 1936 and first discovered by Hewish et al. in 1968 [15, 16]. The study of the interior of the neutron star is a puzzle of special interest to nuclear physicists and astrophysicists because they are one of the densest objects in the universe with a radius of the order of 10 K.M. and mass lower than 2.16M$\odot$ (M$\odot$ = Solar Mass) [17].

A star is the home of thermonuclear fusion in its core like that of sun. The energy

released in this process generates the thermal pressure to sustain against gravitational collapse. During the stellar evolution, synthesis of elements with the lower mass number takes place and it stops once the core become iron-rich, and the fuel gets exhausted. At this stage, the core is supported by electron degeneracy pressure alone. The core collapse takes place when this pressure is not sufficient, and protons and electrons combine through electron-capture into neutrons resulting in an enormous release of neutrinos. Thus, the core becomes more neutron-rich, and collapse gets halted at nuclear density due to the repulsive core. As a result, a shock wave is generated which starts travelling from crust to core leading to core-collapse supernova. The remnant left is called the neutron star. This remnant can also be a stellar black hole if its mass exceeds $5M\odot$.

The core collapse supernova or CCSN is a remarkable phenomenon which serves as a key to understanding the early universe and its origin. The CCSN releases 3×10^{53} erg energy [18] within seconds and allows us to study phenomena like Quark-Gluon Plasma (QGP) which are otherwise very difficult to reproduce in the laboratory environment. Therefore, it becomes essential to examine the nuclear matter at normal and supernormal density in both situations i.e. zero and at finite temperature regime.

1.4 Equation of State

The equation of state (EoS) is characteristic of a physical, thermodynamic system, which determines the state of the system under specified physical conditions. In general, it is a relationship between the pressure of the system to its energy density and temperature, i.e. $P = P(\epsilon, T)$. The EoS describe the complete profile of the system and is generally derived using various methods of statistical physics considering appropriate interactions. EoS of nuclear matter plays a significant role in determining the Mass-Radius profile of neutron star or hypothetical quark star, which are subsequently used for examining phenomena like gravitational wave strains and merger of two neutron stars [19]. In nuclear matter case, it broadly falls into two categories, namely stiff and soft depending on their high and low incompressibility at saturation (k_∞). A stiff EoS estimates greater mass and radius whereas the soft EoS predicts the lower mass and radius of neutron star [20] as compared to data obtained through various astrophysical measurements [21, 22].

1.5 E-RMF Theory and Evolution of Force Parameters

Quantum chromodynamics (QCD) is fundamental and an elegant local gauge theory for strong interaction between quark and gluons that make up the hadrons. It characterises by colour confinement and asymptotic freedom, i.e., interaction becomes weak at a short distance and very strong at a larger distance. Therefore one can not use it to explain the many-baryon system at large distances or low energies due to its nonperturbative property. Quantum Hadrodynamics (QHD) on the other hand is effective field theory for hadron-hadron interaction and provides a correct description at large distance or low energy. Among these theories, Relativistic Mean Field Theory (RMFT) and most recently developed Effective Relativistic Mean Field Theory (E-RMFT) are the most successful and self-consistent theories in the last four decades. They not only describe the property of finite nuclear system but give exceptional results when applied to the nuclear matter at the supernormal densities and nuclear astrophysical situations such as a neutron star. RMF theory is extensively used to probe the unknown territory of nuclear matter near neutron and proton drip line for the finite systems [23] as well as for astrophysical systems like a core-collapse supernova, quark-gluon plasma and polarisation of gravitational waves etc. [19, 24], whose collective understanding is essential for overall understanding of the universe.

In the RMF theory, mesons are collectively taken as fields and describe the interaction among nucleons. Schiff in 1951 [25] for the very first time investigated the baryon and scalar classical neutral meson field using relativistic field theory. Johnson and Teller in 1955 [26] subsequently developed this idea and found the scalar field to be a relevant degree of freedom for describing many empirical features of the nuclear structure. In 1956, Düerr [27] further refined the idea and observed that finite nuclei properties like spin-orbit interaction could be deduced after inclusion of vector meson and using this suggestion in 1974, the first systematic and successful model was developed by including only scalar σ and vector ω mesons called Walecka model [14]. This model estimates the binding energy -15.75 MeV with Fermi momentum k_F^0 =1.42 fm^{-1}. The EoS described by this model meanwhile records unreasonable incompressibility at saturation $K_\infty \approx 550$ MeV which is quite high as estimated by monopole resonance experimental data of 240

$\pm$ 20 MeV [22]. This model also gives a stiff EoS, and therefore, a series of parameter sets were introduced such as NL1, NL2 [28] and NL3 [29] which included ρ meson to take care of the neutron-proton asymmetry and self-couplings of σ meson to reduce the incompressibility to a considerable value. The NL3 set is one of the most used parameters set for finite nuclear matter, and it gives phenomenal results for properties like charge radius and quadruple deformation for most of the elements in the periodic table which include nuclei away from the valley of stability as well [30]. The NL3 still has $K_\infty \approx$ 271.33 MeV which account for a stiff EoS at supernormal density. The incompressibility is further reduced by the addition of vector self-coupling ζ_0 and several parameter sets were designed which explained the behaviour of finite nuclei excellently well [31]. For the first time, cross-coupling (Λ_ω) of ρ meson and the ω meson was introduced by Todd-Rutel and Piekarewicz [32] in context to neutron star radius and neutron skin thickness. This coupling can be considered a bridge between relativistic and non-relativistic formalism.

Furnstahl, Serot and Tang [33] refined the conventional RMF theory and developed Effective Mean-Field Theory for nuclear interaction where they used all the couplings up to the fourth order in agreement with the naturalness and naive Dimension analysis [34]. They introduced sets such as G1 and G2. These parameter sets based on E-RMF formalism give soft EoS both at high density and about saturation. These are consistent with the experimental data of measurement of kaon production and recent neutron star observations of the prediction of mass M $\approx 2.1 M_\odot$ [35].

1.6 Why Relativistic Formalism?

It is a very well known fact that nuclear force is the most strange force known to humanity and strong interaction is not yet fully understood, unlike electromagnetic interaction. Also, probing a nuclear system with several nucleons with a theory based on the first principle is somewhat unrealistic and impossible analytically and numerically. Therefore, nuclear physicist developed several models and theories based on experimental data. They explained the properties of nucleus exceptionally well. For example, the Shell model predicts the magic numbers remarkably, although its success is not understood precisely as unlike atomic shells, nucleon does not have a charge centre. All these models and theories are non-relativistic where static potentials fit to two-body scattering data are

inserted in the Schrödinger equation considering the strength of the potential -50 MeV which is much less than the rest mass of nucleons $\approx$ 939 MeV.

Although the success of non-relativistic nuclear physics has no parallel, it does lack some intricacies which are necessary to investigate the system for a complete and comprehensive picture of nuclear force and its behaviour. Relativistic nuclear physics and in present case RMF theory on the other hand best describe the nuclear matter system at any instance. The relativistic theory has the upper hand considering our system of interest like Neutron Star which can only be described with relativistic formalism. Apart from this, the need to have a relativistic nuclear theory can be discussed as follows.

- The RMF theory based on Dirac phenomenology takes into account the spin-orbit interaction automatically as the $l{\cdot}s$ coupling is purely a relativistic quantum mechanical phenomena, whereas non-relativistic cases insert this term externally in the Schrödinger equation. Moreover, The -50 MeV strength of potential is the sum of two large potential terms (scalar (S $\approx$ -400 MeV) and vector (V $\approx$ 350 MeV) [36]) which accounts for attractive and repulsive nature of nuclear force. Therefore, the fields acting on nucleons are comparable to their rest mass and relativistic effect cannot be neglected.

- The direct consequence of the relativistic effect can be observed from anomalous $l{\cdot}s$ splitting in nuclear sublevels. The splitting is $\approx$ 30 times stronger to its atomic counterpart and has opposite sign [37].

1.7 Phase Transition

A physical system at any instance is characterised by the associated thermodynamic function which is generally a variable in temperature, pressure and density. Sometimes, we encounter a discontinuity or singularity in the thermodynamic function of a given system which corresponds to various kinds of phase changes in the system such as melting and condensation. Examining nuclear matter as a function of these thermodynamical variables is one of the most challenging problems in nuclear physics. The main aim of heavy ion induced collision dynamics is to validate the phase transformation phenomenon on the theoretical as well as the experimental front. The phase change of nuclear matter at near nuclear density is analogous to the liquid-gas phase transition and at the supernormal

density, it becomes Quark-Gluon Plasma (QGP) which is the laboratory for astrophysicists to reveal the deepest secrets of the universe. This is shown in Fig. 1.1 where our present understanding of the nuclear matter phase diagram is represented.

It is well known that at normal density ρ_0 $\approx$0.15 fm^{-3}, nuclear matter shows Van der Waals behaviour. As one increases the temperature, nuclear matter evaporates and undergoes the first order phase transition just as in case of water where latent heat of vaporisation is involved [38]. It remains in two-phase coexistence until a critical temperature T_c is reached after which the system can only exist in the gaseous phase [39]. In the phase space diagram, the slope becomes zero at this temperature. In the laboratory, the only way to give such an enormous temperature (1eV= 11,600K) is by heavy ion induced multi-fragment reactions and compound nucleus reaction. In heavy-ion reaction, one nucleus is accelerated with very high velocity and is made to collide with another nucleus. This reaction can also proceed with the formation of a compound nucleus, in which one nucleus coleuses with others with a lifetime of $\approx 10^{-15}$ s. The phase change can also be found in the crust of neutron star where density approaches the nuclear density.

The idea that nuclear matter can show critical behaviour was given by Mahi et al. [40] and Finn et al. [41]. They performed multi-fragment Proton-Xenon reaction to analyse the variation of mass with yield. The idea was tested several times in subsequent years with multiple experiments [42, 43]. Therefore, several authors have performed numerous theoretical calculations of nuclear matter at finite temperature regime. The theoretical calculations have been performed by various non-relativistic approaches such as Thomas-Fermi model [44], Hartree-Fock theory [45], Skyrme and Gogny interaction [46]. They predicted the critical temperature in the range of 15-20 MeV [47]. These calculation have also been performed in the relativistic domain using RMF theory, and it estimates the critical temperature in range 14.2-16.1 MeV [48].

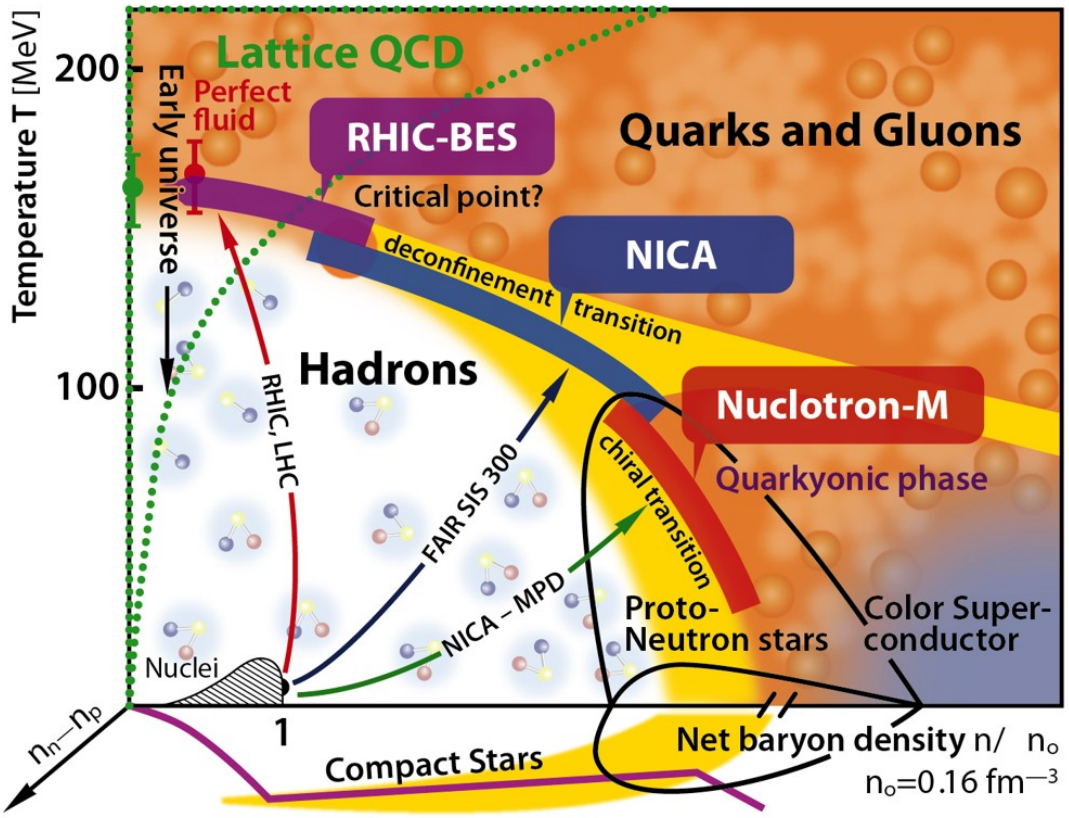

Figure 1.1: Present Understanding of Nuclear Matter Phase Diagram [49].

The dissertation is organised as follows: A brief description of RMF theory at zero temperature and its extrapolation to finite temperature limit is discussed in chapter 2. The versatility and thermodynamic consistency of the RMF theory is also discussed. In chapter 3, the equation of state using various parameter sets has been obtained and is compared with the available data. Various properties of symmetric and asymmetric nuclear matter are discussed in context to the used parameter sets. Chapter 4 is devoted to the RMF theory at finite temperature limit. The liquid-gas phase transition is discussed for both symmetric and asymmetric nuclear matter in view of recently developed force parameter G3, FSUGarnet and IOPB-I. The significance of scalar and vector coupling is investigated for finite temperature case. Summary and concluding remarks are briefed in chapter 5. The future scope and possible extension of present work are also discussed in this chapter.

Chapter 2

Formulation and Methodology

Effective Relativistic Mean Field (E-RMF) theory is an "effective field theory" of strong interaction at low energies. The excellence of this theory is that it takes care of spin-orbit interaction automatically and one need not worry about renormalisation and divergence of the system [33]. It is a relativistic generalisation of Hartree-Fock-Bogoliubov theory of one boson exchange interaction potential (OBE) [50]. In an effective nuclear theory, there are infinite number of terms in Lagrangian and none can be dropped without proper symmetry argument. Therefore, a truncation scheme is usually adopted for possible solutions, and the ratio of meson fields to the mass of nucleon is used for this purpose as this ratio is always less than unity [51]. In the E-RMF theory, nucleons are considered to oscillate in the mean field created by the exchange of mesons and photons. The nucleons are Dirac particle and interact with isoscalar-scalar σ (J^P, T) = (0^+, 0), isoscalar-vector ω (1^-, 0) and isovector-vector ρ (1^-, 1) mesons. It then exploits the naive dimension analysis and naturalness constraints to remove ambiguities in the expansion, i.e. the dimensionless coupling constants should approximately be 1 [30]. The theory also preserves the fundamental symmetries arising in the quantum chromodynamics (QCD) which makes it the most successful theory in nuclear physics for over four decades. Finally, the coupling constants and mass of σ meson are calibrated using the experimental value of ground state property of some known spherical and deformed nuclei.

2.1 E-RMF at Zero Temperature

The basic E-RMF Lagrangian for nucleon-meson interaction as used by Furnstahl et al. [33] with σ, ω, ρ, δ meson and photon coupling with Dirac nucleons and their cross

couplings up to the fourth order is written as [52]

$$\begin{aligned}\mathcal{E} &= \psi^{\dagger}(i\alpha.\boldsymbol{\nabla} + \beta[M - \Phi(r) - \tau_3 D(r)] + W(r) + \frac{1}{2}\tau_3 R(r) + \frac{1+\tau_3}{2}A(r) \\ &- \frac{i\beta\alpha}{2M}(f_\omega \boldsymbol{\nabla} W(r) + \frac{1}{2}f_\rho \tau_3 \boldsymbol{\nabla} R(r)))\psi + \left(\frac{1}{2} + \frac{k_3\Phi(r)}{3!M} + \frac{k_4}{4!}\frac{\Phi^2(r)}{M^2}\right)\frac{m_s^2}{g_s^2}\Phi(r)^2 \\ &- \frac{\zeta_0}{4!}\frac{1}{g_\omega^2}W(r)^4 + \frac{1}{2g_s^2}\Big(1 + \alpha_1\frac{\Phi(r)}{M}\Big)(\boldsymbol{\nabla}\Phi(r))^2 - \frac{1}{2g_\omega^2}\Big(1 + \alpha_2\frac{\Phi(r)}{M}\Big)(\boldsymbol{\nabla}W(r))^2 \\ &- \frac{1}{2}\Big(1 + \eta_1\frac{\Phi(r)}{M} + \frac{\eta_2}{2}\frac{\Phi^2(r)}{M^2}\Big)\frac{m_\omega^2}{g_\omega^2}W^2(r) - \frac{1}{2e^2}(\boldsymbol{\nabla}A^2(r))^2 - \frac{1}{2g_\rho^2}(\boldsymbol{\nabla}R(r))^2 \\ &- \frac{1}{2}\Big(1 + \eta_\rho\frac{\Phi(r)}{M}\Big)\frac{m_\rho^2}{g_\rho^2}R^2(r) - \Lambda_\omega(R^2(r)W^2(r)) + \frac{1}{2g_\delta^2}(\boldsymbol{\nabla}D(r))^2 + \frac{1}{2}\frac{m_\delta^2}{g_\delta^2}(D(r))^2.\end{aligned} \tag{2.1}$$

Here $\Phi(r)$, W(r), R(r), D(r) and A(r) are the fields corresponding to σ, ω, ρ and δ mesons and photon respectively. The g_s, g_ω, g_ρ, g_δ and $\frac{e^2}{4\pi}$ are the corresponding coupling constants and m_s, m_ω, m_ρ and m_δ are the corresponding masses. This Lagrangian is solved using the Euler-Lagrange equation

$$\frac{\partial\mathcal{L}}{\partial\phi(x)} - \partial_\mu\frac{\partial\mathcal{L}}{\partial\partial_\mu\phi(x)} = 0, \tag{2.2}$$

to obtain field equations for nucleons and mesons within mean-field approximations due to which spatial component of field vanishes and only time like component remains. Also, the time-reversal symmetry and charge conservation guarantees that only the third component of isospin sustains [53]. The Lagrangian multiplier ε_α is then used to obtain the single particle energy of nucleon within normalisation constraint as $\sum_\alpha \psi_\alpha^\dagger\psi_\alpha = 1$ [54]. In the E-RMF theory, the negative energy state does not contribute to the current, and therefore, the no-sea approximation becomes essential for obtaining any stationary state solutions of field equations [28]. The effective mass of the proton and neutron changes because of their motion in the mean potential generated by the mesons. It is given as

$$M_p^* = M - \Phi(r) - D(r), \tag{2.3}$$

$$M_n^* = M - \Phi(r) + D(r). \tag{2.4}$$

To obtain the EoS in pressure and energy density, one envoke the energy-momentum tensor $T_{\mu\nu}$ [55]:

$$T_{\mu\nu} = \partial^\nu\phi(x))\frac{\partial\mathcal{L}}{\partial\partial_\mu\phi(x)} - \eta^{\nu\mu}\mathcal{L}, \tag{2.5}$$

where the zeroth component $T_{00} = H$ corresponds to energy density (E) and the third component T_{ii} gives us the pressure (P) as

$$\begin{aligned} E =& \sum_{p,n} \frac{\gamma}{(2\pi)^3} \int_0^{K_F} \mathrm{d}^3k\, E^*_{p,n}(k) + \rho W + \Big(\frac{1}{2} + \frac{k_3\Phi}{3!M} + \frac{k_4}{4!}\frac{\Phi^2}{M^2}\Big)\frac{m_s^2}{g_s^2}\Phi^2 \\ & - \frac{1}{2}\Big(1 + \eta_1\frac{\Phi}{M} + \frac{\eta_2}{2}\frac{\Phi^2}{M^2}\Big)\frac{m_\omega^2}{g_\omega^2}W^2 - \frac{\zeta_0}{4!}\frac{1}{g_\omega^2}W^4 + \frac{1}{2}\rho_3 R - \frac{1}{2}\Big(1 + \eta_\rho\frac{\Phi}{M}\Big)\frac{m_\rho^2}{g_\rho^2}R^2 \\ & - \Lambda_\omega(R^2W^2) + \frac{1}{2}\frac{m_\delta^2}{g_\delta^2}(D)^2 \end{aligned} \tag{2.6}$$

and

$$\begin{aligned} P =& \sum_{p,n} \frac{\gamma}{3(2\pi)^3} \int_0^{K_F} \mathrm{d}^3k\, \frac{k^2}{E^*_{p,n}(k)} - \Big(\frac{1}{2} + \frac{k_3\Phi}{3!M} + \frac{k_4}{4!}\frac{\Phi^2}{M^2}\Big)\frac{m_s^2}{g_s^2}\Phi^2 \\ & + \frac{1}{2}\Big(1 + \eta_1\frac{\Phi}{M} + \frac{\eta_2}{2}\frac{\Phi^2}{M^2}\Big)\frac{m_\omega^2}{g_\omega^2}W^2 + \frac{\zeta_0}{4!}\frac{1}{g_\omega^2}W^4 + \frac{1}{2}\Big(1 + \eta_\rho\frac{\Phi}{M}\Big)\frac{m_\rho^2}{g_\rho^2}R^2 \\ & + \Lambda_\omega(R^2W^2) - \frac{1}{2}\frac{m_\delta^2}{g_\delta^2}(D)^2. \end{aligned} \tag{2.7}$$

Here γ is the spin-isospin degeneracy and K_F is the Fermi momentum.

2.2 E-RMF at Finite Temperature

The most significant advantage of E-RMF is that it is thermodynamically consistent and follows the relevant viral theorem [38]. Therefore, it is straightforward to extrapolate this theory in the finite temperature regime. To do this, one must have a thermodynamic function of the system which is ensemble average of operators arising in theory. Thus, we define a grand canonical partition function Z which is related to thermodynamic potential Ω as [14];

$$\Omega = -k_B \mathrm{T} \ln Z \tag{2.8}$$

and

$$Z = Tr\Big\{\exp\Big(-\beta(\hat{\mathbf{H}} - \mu\hat{\mathbf{B}})\Big)\Big\}. \tag{2.9}$$

Where Z is the grand canonical partition function, $\hat{\mathbf{H}}$ is the Hamiltonian operator and $\hat{\mathbf{B}}$ is the baryon number operator for the mean field and k_B is the Boltzmann constant. The basic relations between thermodynamic potential (Ω), entropy (S), chemical potential (μ)

and temperature (T) are given by

$$\Omega = -pV = E - TS - \mu B \tag{2.10}$$

and

$$\mathrm{d}\Omega = -S\,\mathrm{d}T - p\,\mathrm{d}V - B\,\mathrm{d}\mu\,. \tag{2.11}$$

Now the baryon and scalar densities can be calculated by using the ensemble average and are given as :

$$\rho_b = \frac{1}{V}\Big[\frac{\partial\Omega}{\partial\mu}\Big] = \sum_\alpha \frac{\gamma}{(2\pi)^3}\int_0^\infty \mathrm{d}^3k[n_k(T) - \bar{n}_k(T)] \tag{2.12}$$

and

$$\rho_s = \frac{1}{V}\Big[\frac{\partial\Omega}{\partial M}\Big] = \sum_\alpha \frac{\gamma}{(2\pi)^3}\int_0^\infty \mathrm{d}^3k\frac{m^*_\alpha}{\sqrt{k^2_\alpha + M^*_\alpha}}[n_k(T) + \bar{n}_k(T)], \tag{2.13}$$

with the $n_k(T)$ and $\bar{n}_k(T)$ as the baryons and antibaryons occupation numbers respectively, which are defined by the Fermi distribution function at finite temperature T as

$$n_k(T) = \frac{1}{1 + \exp\left(\frac{(E^*(k)-\nu)}{T}\right)} \tag{2.14}$$

and

$$\bar{n}_k(T) = \frac{1}{1 + \exp\left(\frac{(E^*(k)+\nu)}{T}\right)}, \tag{2.15}$$

with $\mathrm{E}^* = \sqrt{k^2 + M^{*2}}$. The effective chemical potential ν for proton and neutron in eqns. 2.14 and 2.15 in terms of chemical potential μ are defined as

$$\nu_p = \mu - W(r) + \frac{1}{2}R(r), \tag{2.16}$$

$$\nu_n = \mu - W(r) - \frac{1}{2}R(r). \tag{2.17}$$

The entropy density s ($S = s/\rho_b$) can easily be calculated and has the same form as that for a non-interacting gas. It is given as [56]

$$s_i = -2\sum_i \int_0^\infty \frac{\mathrm{d}^3k}{(2\pi)^3}[n_k \ln n_k + (1-n_k)\ln(1-n_k) + (n_k \leftrightarrow \bar{n}_k)]. \tag{2.18}$$

The energy and pressure expression now can be calculated from energy-momentum tensor $\mathrm{T}_{\mu\nu}$ given in Eq. 2.5 as

$$\begin{aligned} E =& \sum_{p,n} \frac{\gamma}{(2\pi)^3} \int_0^\infty \mathrm{d}^3k\, E^*_{p,n}(k)[n_k(T) + \bar{n}_k(T)] + \rho W + \Big(\frac{1}{2} + \frac{k_3\Phi}{3!M} + \frac{k_4}{4!}\frac{\Phi^2}{M^2}\Big)\frac{m_s^2}{g_s^2}\Phi^2 \\ & - \frac{1}{2}\Big(1 + \eta_1\frac{\Phi}{M} + \frac{\eta_2}{2}\frac{\Phi^2}{M^2}\Big)\frac{m_\omega^2}{g_\omega^2}W^2 - \frac{\zeta_0}{4!}\frac{1}{g_\omega^2}W^4 + \frac{1}{2}\rho_3 R - \frac{1}{2}\Big(1 + \eta_\rho\frac{\Phi}{M}\Big)\frac{m_\rho^2}{g_\rho^2}R^2 \\ & - \Lambda_\omega(R^2W^2) + \frac{1}{2}\frac{m_\delta^2}{g_\delta^2}(D)^2 \end{aligned} \tag{2.19}$$

and

$$\begin{aligned} P =& \sum_{p,n} \frac{\gamma}{3(2\pi)^3} \int_0^\infty \mathrm{d}^3k\, \frac{k^2}{E^*_{p,n}(k)}[n_k(T) + \bar{n}_k(T)] - \Big(\frac{1}{2} + \frac{k_3\Phi}{3!M} + \frac{k_4}{4!}\frac{\Phi^2}{M^2}\Big)\frac{m_s^2}{g_s^2}\Phi^2 \\ & + \frac{1}{2}\Big(1 + \eta_1\frac{\Phi}{M} + \frac{\eta_2}{2}\frac{\Phi^2}{M^2}\Big)\frac{m_\omega^2}{g_\omega^2}W^2 + \frac{\zeta_0}{4!}\frac{1}{g_\omega^2}W^4 + \frac{1}{2}\Big(1 + \eta_\rho\frac{\Phi}{M}\Big)\frac{m_\rho^2}{g_\rho^2}R^2 \\ & + \Lambda_\omega(R^2W^2) - \frac{1}{2}\frac{m_\delta^2}{g_\delta^2}(D)^2. \end{aligned} \tag{2.20}$$

Here γ is the spin-isospin degeneracy. The representation of the density of nuclear matter and asymmetry term is of huge importance. It is given by asymmetric parameter as $\alpha = \frac{\rho_n - \rho_p}{\rho_n + \rho_p}$.

The symmetric matter is represented by $\alpha = 0$ with proton fraction $y_p = 0.5$ and for pure neutron matter $\alpha = 1$ and proton fraction is $y_p = 0$.

Chapter 3

Equation of State at Zero Temperature

A large number of force parameter sets have been formulated since the beginning of Quantum Hadrodynamics (QHD) . Each of these parameter set is designed and calibrated according to the nature of problem. These sets are used by fitting the coupling constants and the mass of sigma (σ) meson to known experimental data. In this chapter we will emphasise on the relevance and versatility of parameter sets used for the calculations.

3.1 Force Parameters

The force parameters used in this work are newly developed FSUGarnet [57], IOPB-I [50], G3 [58] and one of the oldest and widely used NL3 [29] sets. As discussed earlier, the non-linear sets such as NL1 and NL2 have unreasonable incompressibility, and therefore these sets were developed to explain various properties of nuclear matter keeping the incompressibility comparable to the experimental value obtained from isoscalar giant monopole resonance (ISGMR) [22]. The coupling constants for these sets are given in Table 3.1. These parameters are very successful for both finite and infinite matter limits. The NL3 set is known to work remarkably well for finite nuclei calculations and describe properties like quadruple deformation and the charge radius nicely despite its slightly larger incompressibility. The IOPB-I and FSUGarnet force parameters also satisfy the empirical data [34]. Both have bulk matter coupling η_1 and η_2 zero and keep the value of self-coupling ζ_0 of vector ω meson to the suitable limit. These couplings along with scalar self couplings k_3 and k_4 are essential in determining the success of any parameter set. One always try to keep k_4 positive and not very large ζ_0 value in order to get results close to experimental data. Apart from these, each coupling constant in these sets have their importance. For example, the k_3 and k_4 scalar self-coupling take care of 3N interaction

and incompressibility at saturation [59].

	FSUGarnet [57]	IOPB-I [50]	G3 [58]	NL3 [29]
m_s/M	0.529	0.533	0.559	0.541
m_ω/M	0.833	0.833	0.832	0.833
m_ρ/M	0.812	0.812	0.820	0.812
m_δ/M	0.0	0.0	1.043	0.0
$g_s/4\pi$	0.837	0.827	0.782	0.813
$g_\omega/4\pi$	1.091	1.062	0.923	1.024
$g_\rho/4\pi$	1.105	0.885	0.962	0.712
$g_\delta/4\pi$	0.0	0.0	0.160	0.0
k_3 (fm^{-1})	1.368	1.496	2.606	1.465
k_4	-1.397	-2.932	1.694	-5.688
ζ_0	4.410	3.103	1.010	0.0
η_1	0.0	0.0	0.424	0.0
η_2	0.0	0.0	0.114	0.0
η_ρ	0.0	0.0	0.645	0.0
Λ_ω	0.043	0.024	0.038	0.0
α_1	0.0	0.0	2.000	0.0
α_2	0.0	0.0	-1.468	0.0
$f_\omega/4$	0.0	0.0	0.220	0.0
$f_\rho/4$	0.0	0.0	1.239	0.0
β_σ	0.0	0.0	-0.087	0.0
β_ω	0.0	0.0	-0.484	0.0

Table 3.1: The newly developed parameter sets FSUGarnet, IOPB-I, G3 and mostly used NL3 sets. The nucleon mass M is taken as 939 MeV. Coupling constants are dimensionless if not mentioned.

3.2 Infinite Nuclear Matter Properties and Results

As we know that in E-RMF formalism interaction of nucleons with mesons is governed by the Dirac equation with the static scalar and vector potential. These can be written from Eqn. 2.1 as

$$U_S = \Phi(r) \tag{3.1}$$

$$U_V = W(r) + \tfrac{1}{2}\tau_3 R(r) + \tfrac{1+\tau_3}{2} A(r) \tag{3.2}$$

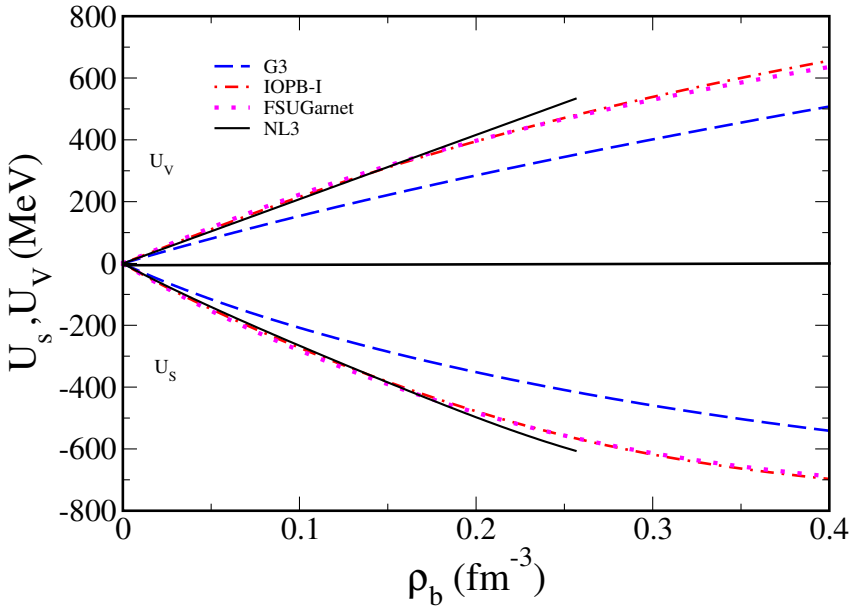

Figure 3.1: The Scalar U_S and Vector U_V potential for the various parameter sets.

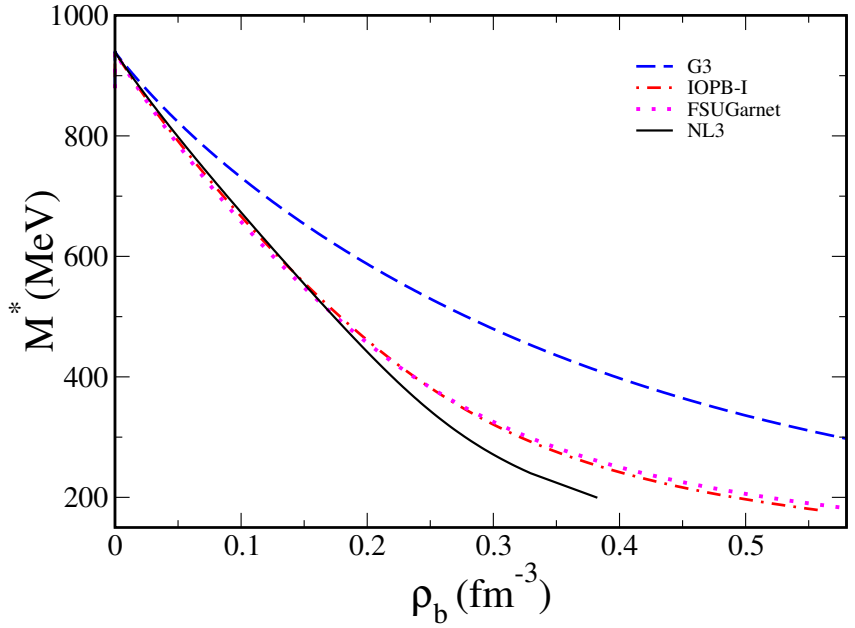

Figure 3.2: Effective Masses of nucleon with baryon density for Symmetric Nuclear Matter.

The Scalar and Vector potentials for symmetric nuclear matter (SNM) as a function of baryon density are displayed in Fig. 3.1 for the four parameter sets as given in Table 3.1. In all the four cases, the vector potential increases linearly in starting and becomes strongly repulsive at higher density as it does not depend on higher order term of vector ω meson. The FSUGarnet, IOPB-I and G3 parameter sets underestimate the potential as predicted by the NL3 set. The IOPB-I and FSUGarnet behave almost the same due to

their similar structure of couplings. The scalar density also follows a similar trend. From the Fig. 3.1 it is also quite clear that the value of these potentials at saturation density ≈ 0.15 fm^{-3} is comparable to nucleon masses which determine the depth of the potential and therefore their relativistic investigation becomes important.

The reason that NL3 set overestimates the potential can be understood effectively from the effective mass versus baryon density curve for SNM as depicted in Fig. 3.2. The effective masses determined from Eq. 2.3 chooses the value of scalar and vector potential through self-consistent equation for scalar density [50]. The NL3 parameter set shows the steepest slope and G3 the least, which directly implicate their trend of potential in Fig. 3.1. The IOPB-I and FSUGarnet sets lie in between these two.

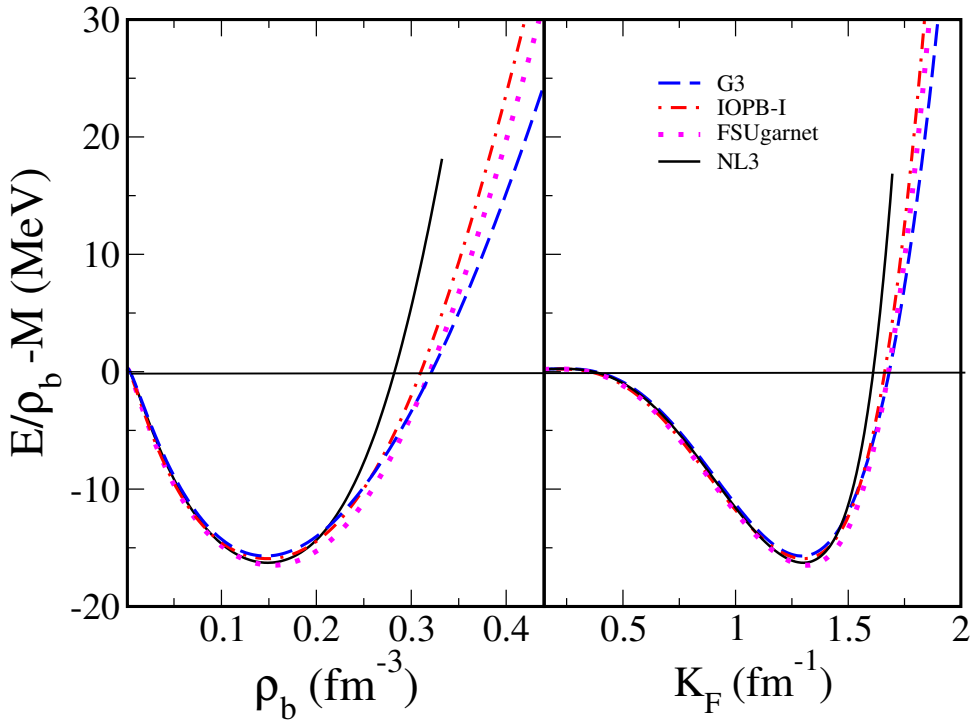

Figure 3.3: Binding Energy as a function of (a) baryon density (b) Fermi momentum.

In Fig. 3.3 the binding energy per nucleon with baryon density and Fermi momentum is shown for SNM. As discussed this was calculated to be ≈ 15.7 MeV at saturation density of ≈ 0.15 fm^{-3} and $K_F^0 = 1.42$ fm^{-1} considering nuclear matter as Fermi degenerate gas [14]. The figure now depicts the stiffness of NL3 set and softness of G3 parameter. Due to this reason, the NL3 set is not preferred at supernormal densities. The value of Binding energy, effective mass, incompressibility and saturation density for these parameters is given in Table 3.2.

	FSUGarnet	IOPB-I	G3	NL3
ρ_0 (fm^{-3})	0.153	0.149	0.148	0.148
M^*/M	0.578	0.593	0.699	0.595
$\mathcal{E}_0$ (MeV)	-16.23	-16.10	-16.02	-16.29
K$_F^0$ (fm^{-1})	1.32	1.30	1.30	1.30
K_∞ (MeV)	229.5	222.65	243.96	271.38

Table 3.2: The Nuclear Matter Properties at Saturation.

Next, we show the binding energy per nucleon versus baryon density for pure neutron matter (PNM) in Fig. 3.4. The four parameter sets have been compared with the data obtained from (NN) and (3N) chiral interaction at high density [60] and microscopic calculation by Friedman et al. [61] at low density. The NL3 set deviates from these data at both low and high density. The G3, IOPB-I and FSUGarnet on the other hand, are consistent with experiments at both density regions. It is to be noted that for pure neutron matter (PNM), the R(r) field comes into effect (see Eqn. 2.1 and reference [50] for field equation) and ω-ρ cross coupling becomes important at low density.

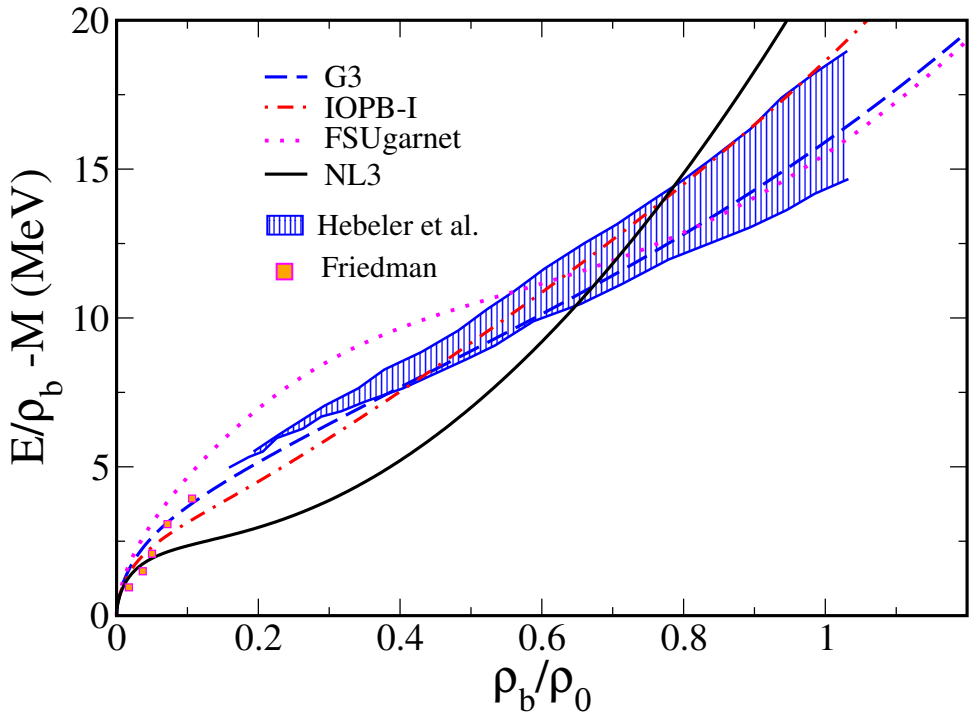

Figure 3.4: The binding energy per nucleon versus baryon density with different E-RMF sets. The shaded region and box corresponds to microscopic calculations by Hebeler [60] method and Friedman [61].

Generally, a neutron star is not merely composed of neutrons. During the evolution of a star, the reactions between hadrons take place, and any photon and neutrino produced escape out resulting in the cooling of the star. In this process, some quantum numbers like baryon number and charge are conserved on a time scale longer compared to the evolution of star and some like strangeness are violated at a shorter time scale [62]. Therefore, there are many species of hadrons and lepton inside a neutron star which are always in chemical equilibrium and maintain the charge neutrality [63]. As a consequence, the matter is ≈ 90 % neutrons and ≈ 10% leptons and proton. Thus it becomes essential to study the EoS for asymmetric nuclear matter. Asymmetry is defined by $\alpha = \frac{\rho_n - \rho_p}{\rho_n + \rho_p}$, where ρ_n and ρ_p corresponds to neutron and proton density respectively.

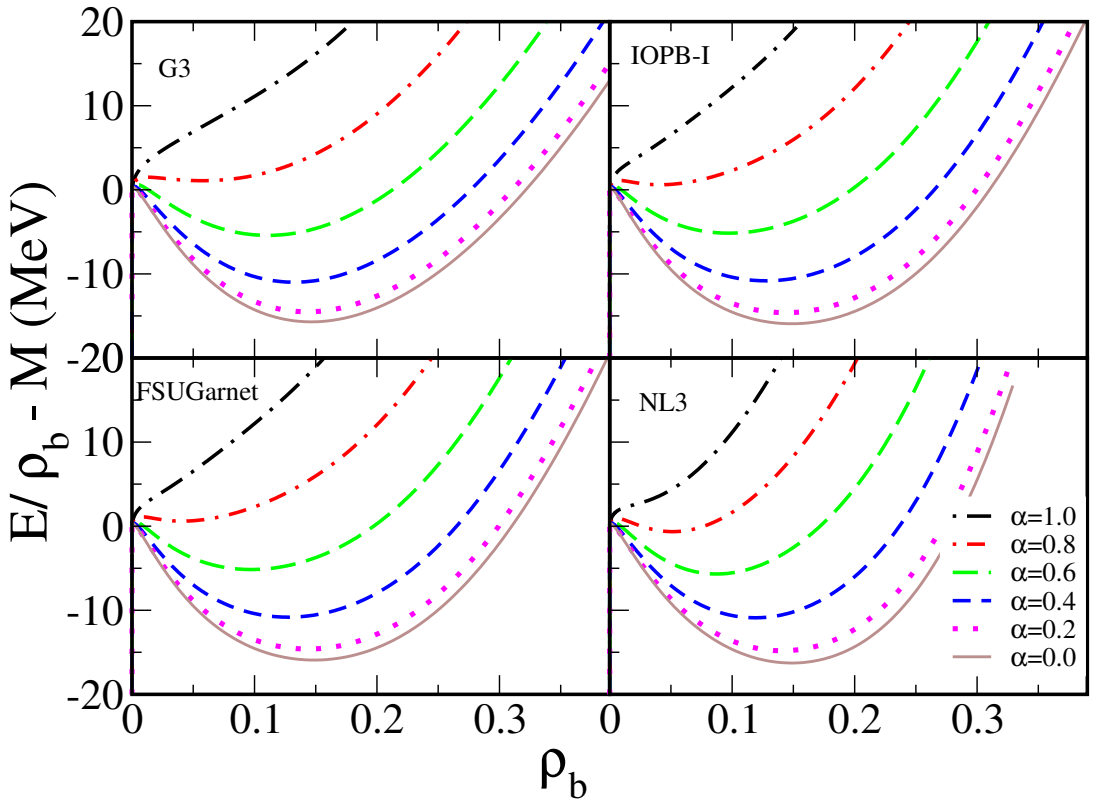

Figure 3.5: The binding energy versus baryon density for the NL3, FSUGarnet, IOPB-I and G3 parameter sets at T = 0 at different α.

The Fig. 3.5 shows the Binding energy as a function of baryon density for the NL3, IOPB-I, G3 and FSUGarnet parameter sets at different asymmetric parameter α. The symmetric nuclear matter that corresponds to $\alpha = 0.0$ or proton fraction $y_p = 0.5$ is well bound at the saturation density. This boundness gets weaker as the asymmetry is increased. As one reaches the pure neutron matter, i.e. $\alpha = 1.0$ or proton fraction

$y_p = 0.0$ the pocket and hence the bound state disappears. Therefore, pure neutron matter is not stable as a neutron mean lifetime is 881.5 $\pm$ 1.5 s [64]. In star, this is always in a beta equilibrium condition with protons and leptons and in the high-density region like core with baryon octet species as well.

For asymmetric matter, the role of δ and ρ meson becomes important to describe nuclear properties in extreme conditions. The origin for these mesons lies in isospin density, but ρ meson arises due to asymmetry in density and δ meson find its source in mass asymmetry. As in Eqn. 2.3, the δ meson split the effective mass of nucleon. The effect can be seen in case of G3 parameter which estimates the softest EoS for neutron matter (PNM) as compared to others. The δ meson and therefore the G3 parameter set is known to describe properties like two-neutron separation energy S_{2n}, neutron-skin thickness and giant monopole resonance [30, 50, 19, 63].

The force parameter set NL3 is exceptionally successful in explaining nuclear properties near nuclear density. The IOPB-I, FSUGarnet and G3 set also have been successfully used for finite nuclear matter properties not only for β equilibrium nuclei but also to the nuclei near proton and neutron drip line. In case of a neutron star, the density can reach 2-10 times the nuclear density. Therefore, probing these E-RMF parameter sets at those supernormal density becomes essential to estimate the astrophysical properties of these object. The EoS obtained from these sets decides the mass-radius profile of star through Tolman–Oppenheimer–Volkoff (TOV) equation [16] and ultimately help to simulate phenomena like a core-collapse supernova, merging of two neutron star, gravitational wave strain etc. [65].

In Fig. 3.6 the pressure is depicted as a function of baryon density for pure neutron matter (PNM) and symmetric nuclear matter (SNM). The results are compared with the experimental data obtained by examining the transverse and elliptical flow from nucleus-nucleus heavy ion collisions. For PNM, there are two sets of bounds corresponding to HIC-Asy Stiff and HIC–Asy Soft depending on their strong and weak density dependence [66]. It is apparent that NL3 set diverges from both the bound obtained from HIC experimental data. On the other hand, FSUGarnet and IOPB-I parameter sets are in reasonable agreement with the flow data for the PNM. However, they give a stiff EoS in contrast to the G3 parametrisation, which satisfies the experimental EoS excellently. The EoS for SNM at zero temperature is shown in Fig. 3.6b and it is clear that EoS of NL3

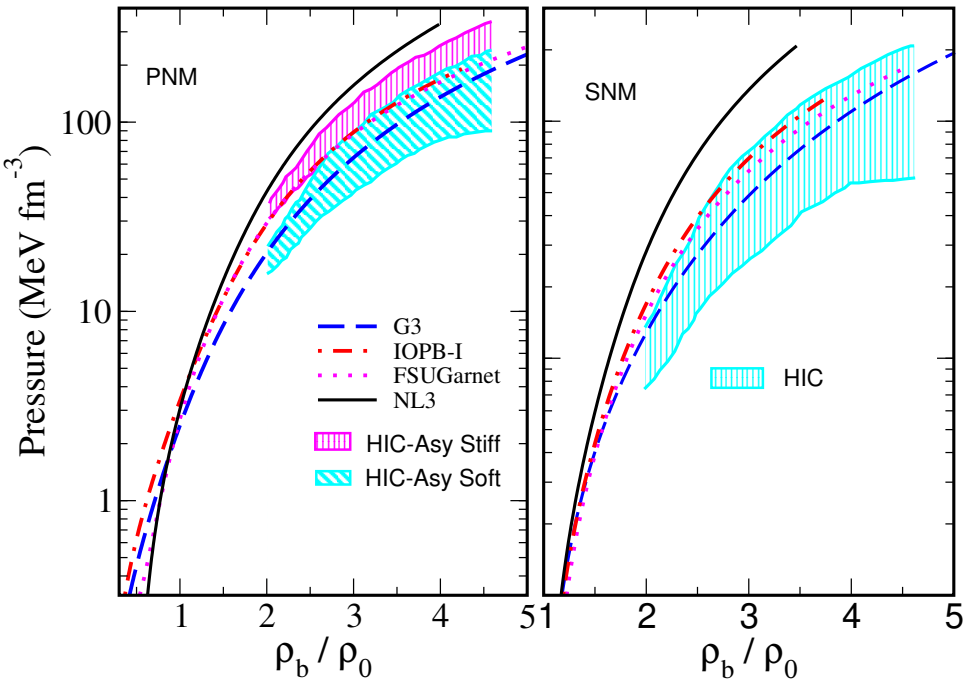

Figure 3.6: The pressure versus baryon density for NL3, FSUGarnet, IOPB-I and G3 parameter sets at T = 0 for (a) pure neutron matter (PNM) and (b) symmetric nuclear matter (SNM). The results are compared with experimental data extracted from analyzing EoS after including pressure from asymmetry and density dependence [66].

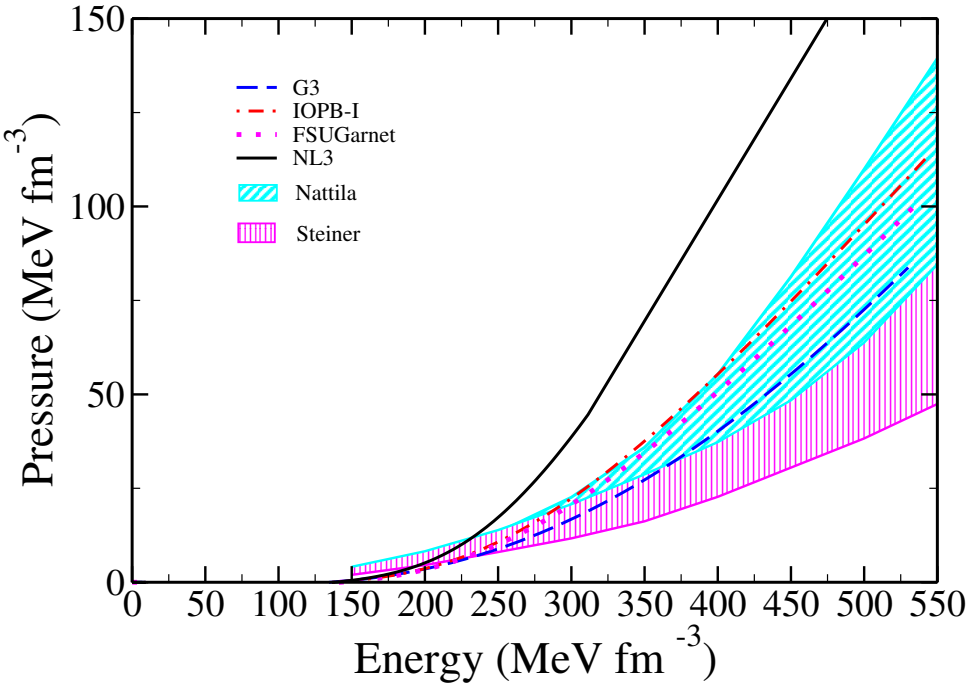

Figure 3.7: The zero temperature equation of state with FSUGarnet, G3, IOPB-I and NL3 sets.. The lower shaded region represents the constraint at r_{ph} =R with a 95% confidence limit. Here r_{ph} and R represents photospheric radius and neutron star radius [67]. The upper shaded region represents the equation of state for zero temperature dense matter with a 95 % confidence limit from QMC + Model A [68].

set deviates from the experimental data drastically. The G3 parameter set satisfies flow data exceptionally well for the entire density range. The other parameter sets, IOPB-I and FSUGarnet, are also consistent with the experimental data from HIC but they give stiffer EoS as compared to G3 force parameter.

The equation of state at zero temperature for symmetric matter is shown in Fig. 3.7. The four parameter sets are compared with experimental data extracted from Steiner et al. [67] and Nättilä et al. [68]. It is evident that the NL3 set yields a stiff EoS and does not follow the experimental trend within the 95% confidence limit. FSUGarnet, IOPB-I and G3 forces are in reasonable agreement with these experimentally derived EoS. The deviation of the mostly used NL3 set lies in the fact that it lacks the vector self and cross-couplings, which inturn weakens the dependence of mesonic field on density. Whereas, the versatility of G3 set can be attributed to its bulk matter couplings ζ_0, η_1 and η_2. The incompressibility in FSUGarnet and IOPB-I is controlled by their vector cross coupling Λ_ω. Although NL3 is giving a stiff EoS, it is the oldest among these parameters and it is one of the most successful forces used in the finite system calculations. It describes nuclear property such as quadruple deformation and the charge radius exceptionally well for most of the periodic table elements [30]. The FSUGarnet and IOPB-I are the recent parameters and reproduces neutron masses in the lower (M=2.06M$\odot$) and upper limit (M=2.15M$\odot$) respectively [19].

3.3 Summary

In summary, it is shown that the Relativistic Mean Field framework is an incredible theory to explain the nuclear matter at both finite and infinite limits. The versatility of the parameter sets, i.e. NL3, FSUGarnet, IOPB-I and G3 is discussed in the context of various nuclear matter properties such as saturation density, binding energy, incompressibility and effective mass etc. The results are compared with the various microscopic as well as astrophysical experiments wherever available, and it is observed that the parameter set used in this work have an extensive range and therefore they can be satisfactorily used for examining the nuclear matter system in extreme conditions as well. We have discussed the importance of σ, ω, ρ and δ meson, their origin and couplings which subsequently describe the symmetric and asymmetric nuclear matter.

Chapter 4

Equation of State at Finite Temperature

In the previous chapter, the RMF formalism at temperature T=0 was briefly discussed. From statistical mechanics, we know that nucleons are fermions and obey the Fermi-Dirac distribution function. The significance of this function is visible at T=0. At absolute zero temperature, the probability of occupation is 1 for a particle with energy less than Fermi energy and zero for energy larger than the Fermi energy. On this principle, the calculation and nuclear matter properties have been discussed. We discussed the nuclear matter within neutron star, but neutron star and a star like Sun is not really at absolute zero temperature. The temperature of the outer core of the sun is 5778 K, and a neutron star has approximately 600000 K of surface temperature. This anomaly can be understood by the fact that the nuclear, and particle physics is based on the natural unit with $\hbar = k{=}c{=}G{=}1$. Therefore the temperature when expressed in MeV, makes those value of temperature almost negligible and hence generally the Sun and a Neutron star are considered cold objects.

The study of nuclear matter at some finite temperature and a density greater than nuclear density form the most challenging problems in nuclear physics. There have been several theoretical models to explain the matter at $T > 0$, but the experiments are not easy to perform due to high computation requirement for reverse kinematics in multi-fragment process. In this work, we are mainly concerned about the phase transition of nuclear matter to hadron gas, i.e. near nuclear density. At higher temperature and density, the Quark-Gluon Plasma is formed as in Fig. 1.1 which is said to be the doorway to understand the universe. The liquid-gas phase transition in the nuclear matter is visible at the core of neutron star where the temperature is little lower and in the laboratory, the environment can be simulated via the heavy ion collision reactions. The main thrust of these experiments is to study the phase transition dynamics. The paramount aim is to

find the critical parameters of phase transition, and it was observed in 2001 from central collisions of Ar^{40} + Sc^{45}, that the critical temperature for this phase transition is 13.0 ± 0.6 MeV [69]. This value was updated recently by two compound nuclear reactions (Ni^{58} + $C^{12} \rightarrow Se^{70}$ and Ni^{64} + $C^{12} \rightarrow Se^{76}$) and four multi-fragment reactions and the critical temperature was found to be 17.9 ± 0.4 MeV [70]. The corresponding critical pressure P_c is 0.31 ± 0.07 MeV/fm^3 and critical density ρ_c is 0.06 ± 0.01 fm^{-3} respectively. This new updated value requires a revisit of theoretical calculations, and an attempt is made here to estimate these critical parameters using the newly developed E-RMF parameter sets whose versatility at T=0 is discussed in the previous chapter.

4.1 E-RMF at T > 0 and Force Parameters

As discussed in the text, the theoretical predictions from all the Non-relativistic approaches estimate the critical temperature to be in the range of 15-20 MeV and the relativistic approaches such as RMF predicts it to be between 14.2-16.1 MeV [48, 47]. These values deviate from the recent experimental data, and therefore, one needs to make changes in the present form of RMF formalism in such a way that it still describe the nuclear matter properties at T=0. The newly developed force parameter IOPB-I, FSUGarnet and G3 along with the mostly used NL3 set are used here at finite temperature calculations and for investigating phase transitions invoking the thermodynamic consistency of E-RMF or Quantum Hadrodynamic (QHD). For the sake of consistency, we imply that the thermodynamic pressure should be equal to hydrostatic pressure derived from stress-energy tensor $T_{\mu\nu}$ i.e T_{ii} or in other words, it should follow the appropriate viral theorem [33]. Moreover, the advantage of a hadronic degree of freedom is that (a) hadrons can be observed experimentally in scattering experiments and calculation can be calibrated accordingly and (b) it is much more efficient at low energy as compared to QCD. We further believe that, since all the force parameter used in this work have different vector meson couplings, they all should behave differently [39]. The formulation as described in chapter 2, is a straightforward extrapolation of the framework at T=0. At finite temperature, the baryons have an infinite number of states to fill, and therefore the integration runs over 0 to ∞ opposite to T=0 case where states up to Fermi energy are allowed.

4.2 Phase Transition in Symmetric Nuclear Matter

The critical temperature, pressure and density mentioned in the text until now are referred to the symmetric nuclear matter (SNM) case. In the symmetric nuclear matter where proton fraction is y_p=0.5, meson corresponding to asymmetry in density and mass, i.e. ρ and δ do not arise. Now with the liquid-gas phase transition analogy, one expects that binding energy should decrease with increase in temperature. This is shown in Fig. 4.1 where binding energy per nucleon obtained as a function of baryon density is shown at different temperatures values.

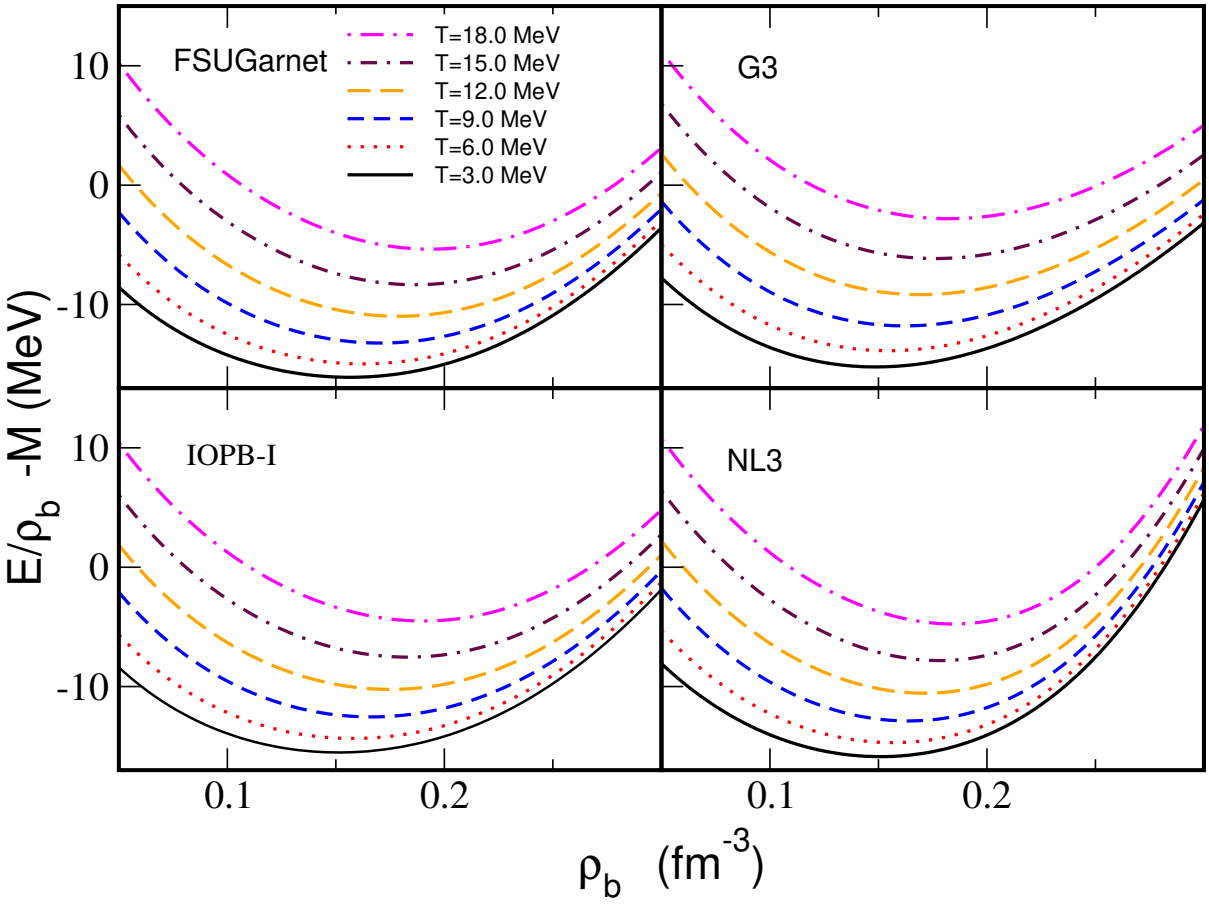

Figure 4.1: The binding energy as a function of baryon density ρ_b at various temperatures for the FSUGarnet, G3, IOPB-I and NL3 sets.

It is apparent that the system tends to become less bound as one increases the temperature and the binding energy keeps decreasing with temperature. The curves around saturation become flat, which signify the softness of EoS. The nuclear density starts increasing with temperature which is common to all the parameter sets. Just as in the case of T=0, G3 estimates the softest EoS at each temperature and NL3 the stiffest.

In a liquid-gas phase diagram, the phase transition is characterised by a non-continuous transition between the two states. This is termed as the first order phase transition, and in general, such phase transition involves the latent heat. Similarly, the nuclear matter undergoes a first order phase transition. The system remains in two-phase coexistence unless a critical temperature is reached after which the system can only exist in the gaseous phase. This transition is marked by an inflation point which is given by [39]

$$\frac{\partial p}{\partial \rho} = \frac{\partial^2 p}{\partial \rho^2} = 0. \tag{4.1}$$

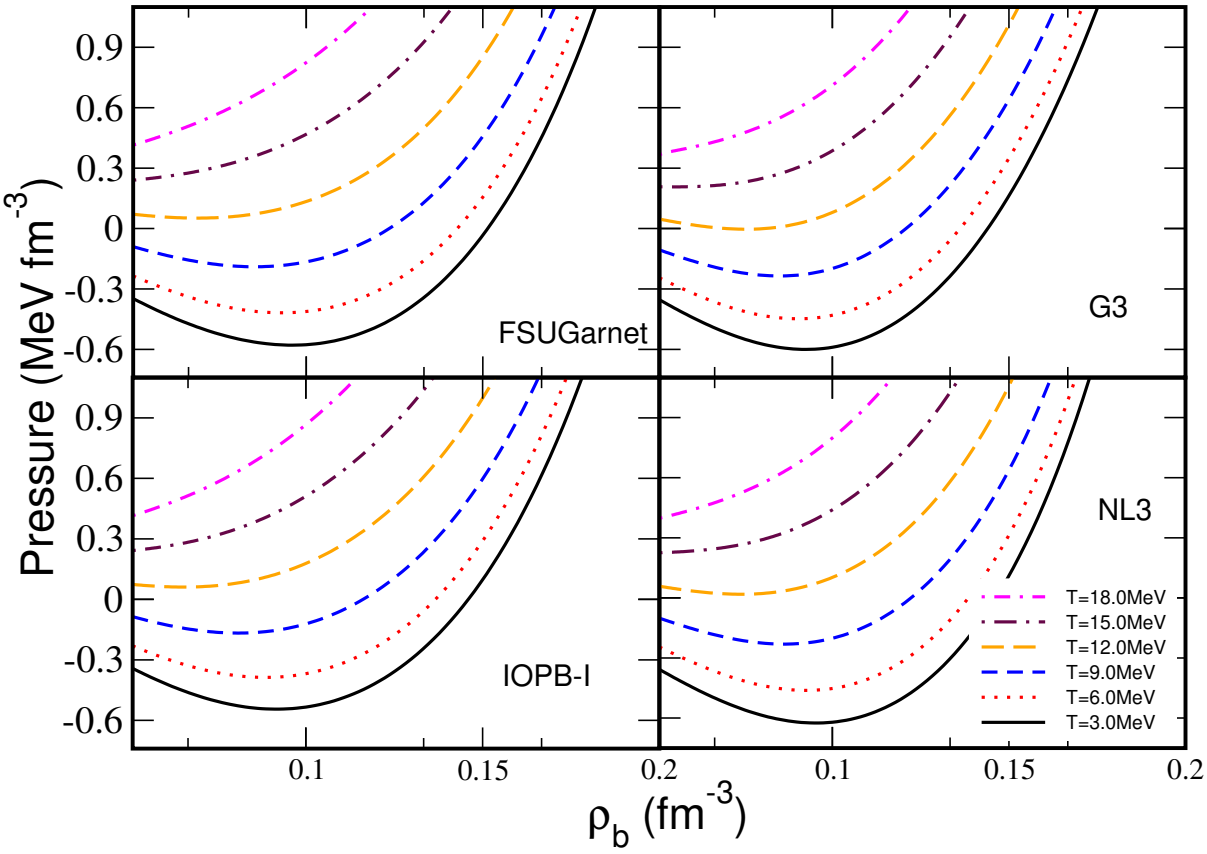

Figure 4.2: The pressure versus baryon density ρ_b at various temperatures for the FSUGarnet, G3, IOPB-I and NL3 sets.

The Fig. 4.2 shows the onset of liquid gas phase transition where the pressure is plotted as a function of baryon density for all the parameter sets. There is a very nice pocket at low temperature signifying the two-phase coexistence which vanishes after the critical temperature T_c is reached. The corresponding pressure and density are also called critical pressure P_c and critical density ρ_c. The estimated values of all these critical parameters along with the various theoretical calculations and experimental results are given in Table

4.1.

	T_c (MeV)	P_c (MeV/fm^3)	ρ_c (fm^{-3})	E/ρ_b at T_c (MeV)
FSUGarnet	13.60	0.1604	0.051	-9.61
IOPB-I	13.60	0.1627	0.048	-8.80
G3	14.30	0.1629	0.062	-6.68
NL3	14.39	0.1913	0.053	-8.38
G1 [35]	14.30	0.1875	0.056	-8.24
G2 [39]	14.30	0.1843	0.043	-8.04
NL1 [71]	13.74	0.1644	0.041	-9.71
NL2 [71]	18.63	0.3616	0.056	-3.47
NL-SH [71]	15.96	0.2644	0.052	-6.70
Exp.1 [70]	17.9 ± 0.4	0.31 ± 0.07	0.06 ± 0.01	-
Exp.2 [69]	13.1 ± 0.6	-	-	-8.0

Table 4.1: The calculated critical temperature T_c (in MeV), critical pressure P_c (in MeV fm^{-3}) and critical density ρ_c (in fm^{-3}) with the respective binding energy (in MeV) at the critical point with FSUGarnet, IOPB-I, G3 and NL3 parameter sets for symmetric nuclear matter. The experimental data are given wherever available.

The parameter sets FSUGarnet, and IOPB-I estimates the T_c to be 13.60 MeV and G3 report it to be 14.30 MeV which is an underestimation if one compares them with the result of experiment 1. These results are comparable to the one obtained from NL3, and another parameter set as given in Table 4.1. Our calculations with the FSUGarnet, IOPB-I and G3 set deviate for T_c and P_c but agree with the critical density and binding energy at saturation.

4.3 Phase Transition in Asymmetric Nuclear Matter

As discussed, the nuclear matter with a neutron star is not symmetric, and if one looks at the core collapse supernova or CCSN, the proton fraction y_p is equal to 0.3 [72]. Therefore, it is essential to examine the phase transition for the asymmetric matter. For the asymmetric matter, the ρ and δ meson coupling appears into effect, and one expects their significant role in determining the property of nuclear matter. As we have seen in

chapter 3 that boundness decreases with an increase in asymmetry (see Fig. 3.5), we expect a similar trend in the finite temperature limit.

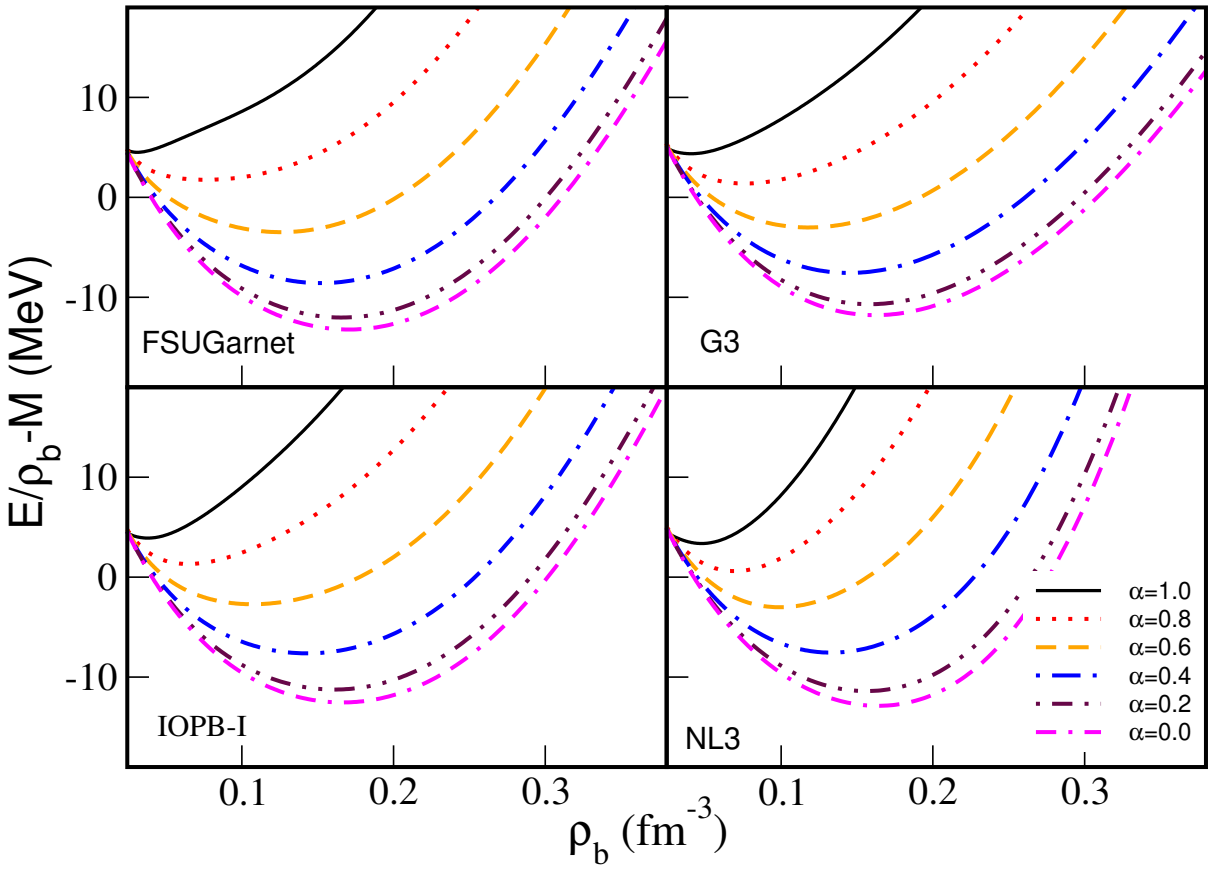

Figure 4.3: The binding energy versus baryon density ρ_b at different $\alpha = \frac{\rho_n - \rho_p}{\rho_n + \rho_p}$ at T=10 MeV for FSUGarnet, G3, IOPB-I and NL3 sets.

Fig. 4.3 shows the binding energy versus baryon density ρ_b for different $\alpha = \frac{\rho_n - \rho_p}{\rho_n + \rho_p}$ FSUGarnet, G3, IOPB-I and NL3 sets at T=10 MeV. We observe the softness from the flatness of curve at the saturation, and it follows the same trend as in case of T=0 with G3 estimating the softest EoS.

The liquid-gas phase transition for the asymmetric matter is portrayed in Fig. 4.4. Here the pressure is plotted as a function of baryon density ρ_b for different asymmetric parameter α. One can distinctly find a deep pocket for SNM, i.e. $\alpha = 0.0$ indicating the two-phase coexistence. This pocket vanishes after $\alpha > 6.0$, and now the pressure increases monotonically with baryon density. For asymmetric matter, we can observe the distinction in the behaviour of FSUGarnet and IOPB-I set as the latter one estimates a sharp rise in pressure as compared to the former after $\alpha > 6.0$. This drift can be attributed to their slightly different ζ_0 value corresponding to vector self-coupling. If we

compare this phase diagram (Fig. 4.4) with the one obtained for T=0 case, i.e. Fig. 4.2, we notice a very sharp rise in pressure in case of the former. This is due to the additional repulsive force arising due to the ρ meson which plays a significant role at higher asymmetry. The ω and ρ meson directly impact the effective chemical potential as in Eq. 2.16. Thus, we can conclude that it is much easier to reach the critical temperature for PNM as compared to SNM.

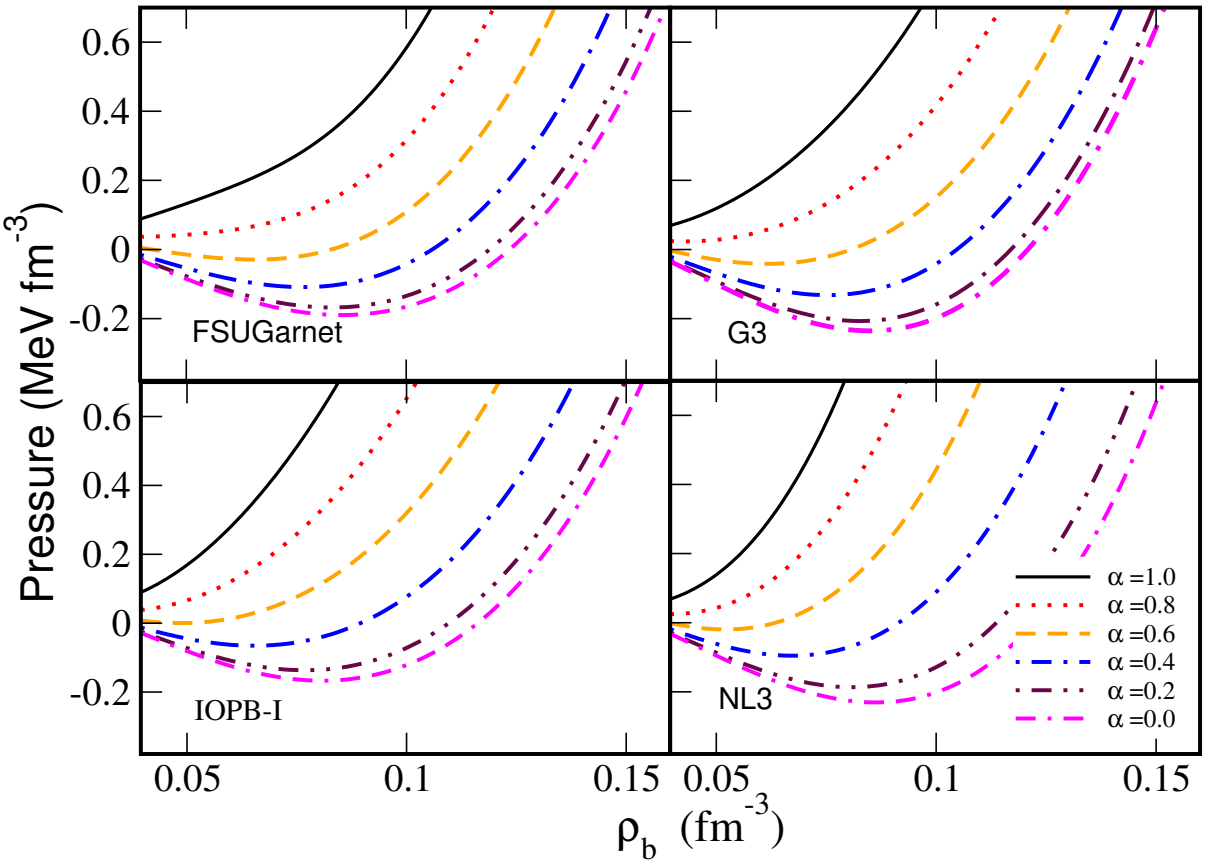

Figure 4.4: The pressure versus baryon density ρ_b for different $\alpha = \frac{\rho_n - \rho_p}{\rho_n + \rho_p}$ at T=10 MeV with the FSUGarnet,G3, IOPB-I and NL3 sets.

The critical asymmetry is plotted in Fig. 4.5 where the critical temperature for the liquid-gas phase transition is plotted against the asymmetry parameter for all the parameter sets. There is a sharp decrease in the critical temperature after $\alpha = 0.6$ for the G3 and NL3 sets whereas, the FSUGarnet and IOPB-I show this behaviour after the asymmetry of $\alpha = 0.7$. This is a direct consequence of extra repulsive force arising due to ω and ρ meson at high asymmetry.

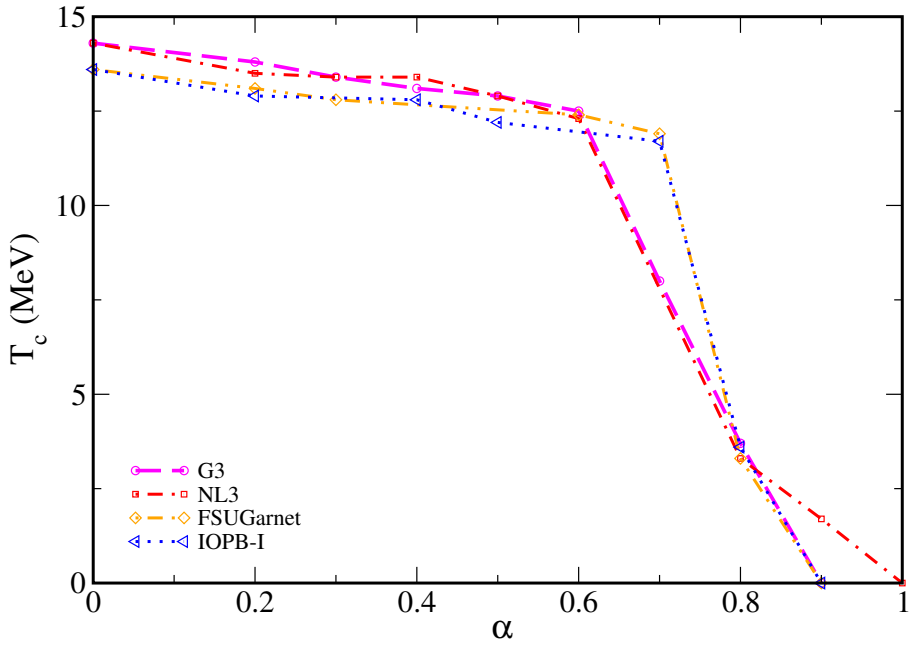

Figure 4.5: The critical temperature T_c versus asymmetry parameter α for the FSUGarnet, G3, IOPB-I and NL3 sets.

4.4 Equation of State (EoS) at Finite Temperature

We now discuss the implication of temperature on EoS. In Fig. 4.6, the effective mass of nucleon for symmetric matter is plotted as a function of baryon density for the parameter set G3.

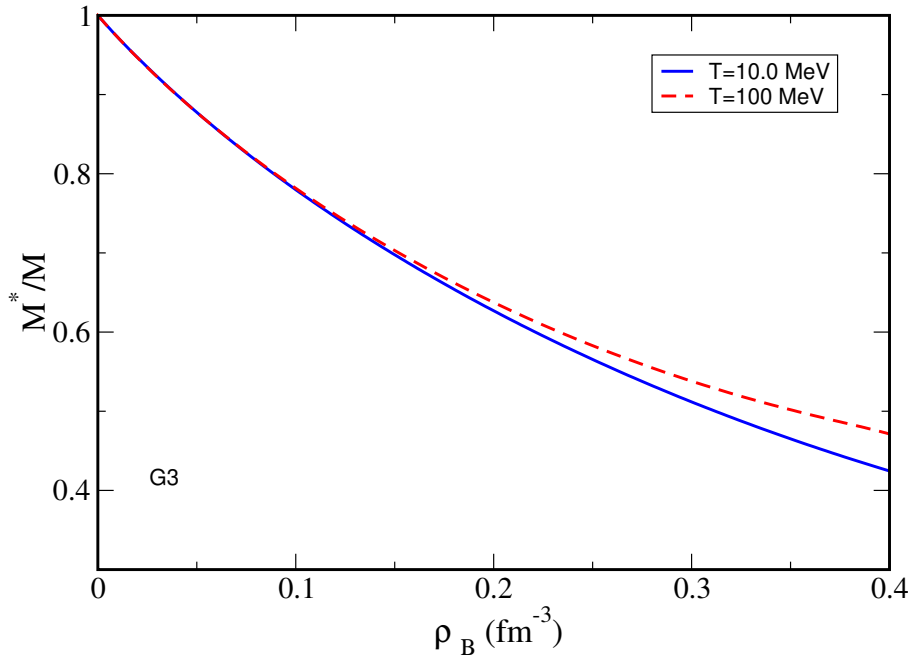

Figure 4.6: The ratio of the effective mass and mass of the nucleon M^*/M versus baryon density ρ_b at T=10 MeV and T=100 MeV for G3.

The effective mass plays a very significant role in determining the EoS which we saw in previous cases as well. When the temperature is increased up to a sufficient level giving rise to the formation of anti-particle, the effective mass increases gradually. The same trend is observed for the rest of the parameter sets as well.

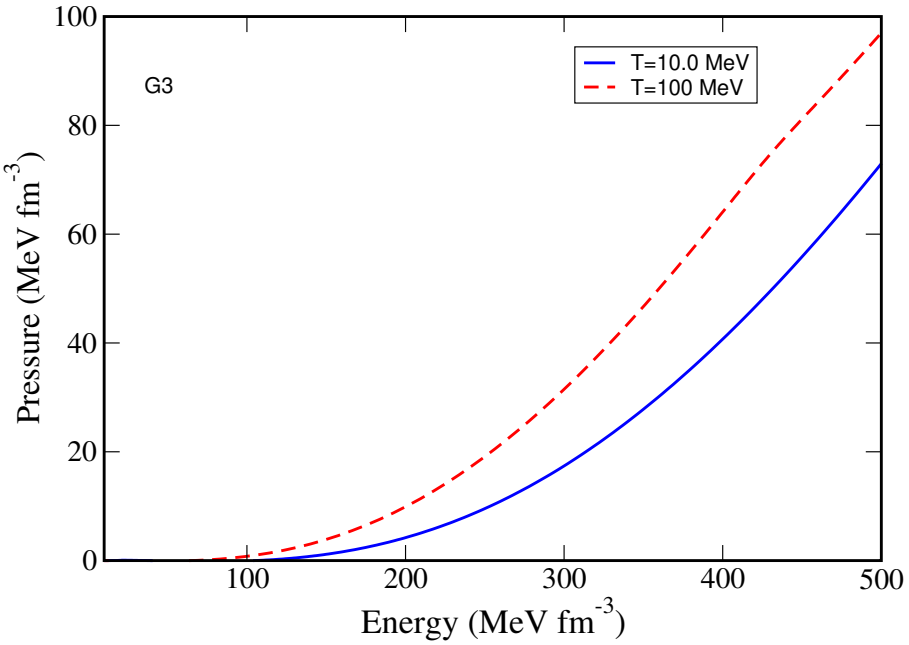

Figure 4.7: Equation of State at T=10 MeV and T=100 MeV for the Parameter set G3.

The increase in temperature makes the EoS stiffer as shown in Fig. 4.7, where the pressure is plotted as a function of the energy density at T=10 MeV and T=100 MeV. At high temperature, anti-baryon production causes extra thermal energy in the system and additional pressure due to increased momentum.

The entropy density which is a function of fermion occupation number as given in Eq. 2.18, is shown in Fig. 4.8 for the parameter set G3 versus baryon density ρ_b. The entropy density decreases exponentially against the baryon density with a larger maximum at larger temperature. At higher temperature, the baryon and antibaryon have infinite states to occupy which increases the randomness. This randomness decreases at lower temperature and high density.

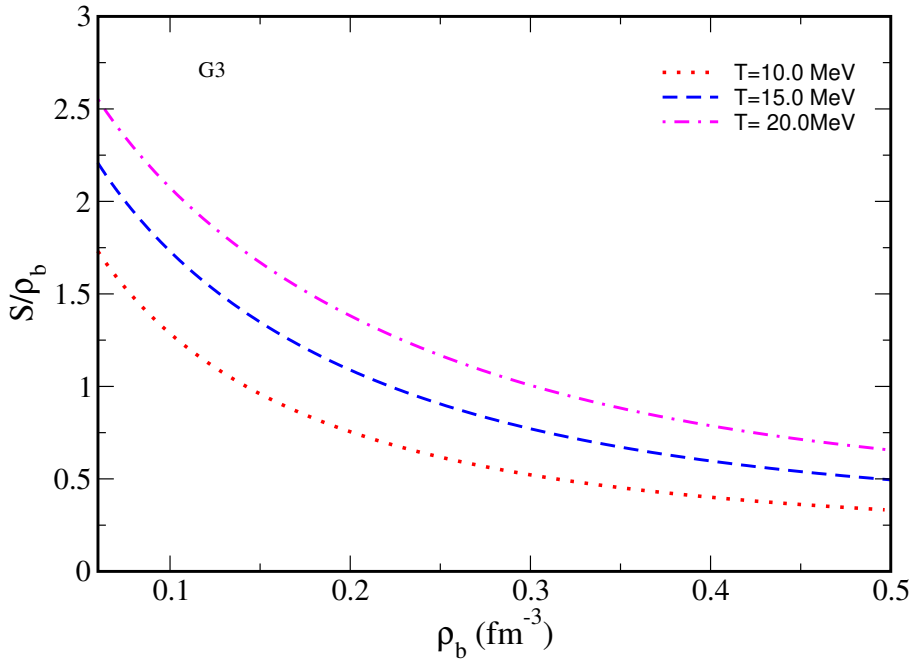

Figure 4.8: The entropy density versus baryon density for the G3 set at different temperatures.

4.5 Summary

In the summary, we have revisited the liquid-gas phase transition problem in the wake of new experiments estimating the value of critical temperature 17.1 ± 0.06 MeV. All present relativistic models including E-RMF parameter sets and non-relativistic models underestimate this value. We have calculated this value along with the critical pressure and density using the newly developed sets FSUGarnet, IOPB-I and G3. In our calculations, the critical temperature lies in the range of 13.6-14.3 MeV. The corresponding critical pressure and density are found to be in the range of (0.16 - 0.19)MeV fm $^{-3}$ and (0.048-0.062) fm^{-3} respectively. We have also investigated the phase transition for asymmetric matter, and the role of vector meson is duly analysed. The critical temperature decreases with an increase in α and pure neutron matter is prone to liquid-gas phase transition at very low temperature. For the asymmetric matter, critical temperature decreases because of the repulsive singlet-singlet and triplet-triplet components of the nuclear force arising from vector ρ meson. The effect of temperature on EoS and effective mass is also addressed. The EoS gets stiffer and effective mass increases as we increase the temperature because of baryon-antibaryon pair formation. Besides this, it is observed that entropy density decreases exponentially with baryon density.

Chapter 5

Summary and Future Scope

5.1 Summary

In this dissertation, we have attempted to investigate the implication of newly developed force parameter sets FSUGarnet, IOPB-I, G3 and often used conventional NL3 set within the Relativistic Mean Field theory at finite and zero temperature limit. This theory is used here to examine various aspects of finite and infinite nuclear matter. The dissertation can be summarised as follows.

Chapter 1: − This chapter contains a brief yet pertinent account of nuclear matter, equation of state, phase transition and Neutron star etc. The Effective Relativistic Mean Field Theory (E-RMF) and the evolution of its parameter sets are briefly described. The importance and requirements of the relativistic treatment of nuclear matter problem are discussed. A brief account of the development of theoretical work on phase transition and its comparison with the experiments is given in this chapter.

Chapter 2: − The detailed formalism of Relativistic Mean Field Theory is given in this chapter. It contains the formalism at temperature T=0 and its extrapolation to finite temperature limit using grand canonical partition function and potential. A brief description of σ, ω, ρ and δ meson and mean field approximation is provided in this chapter. Its relation to the fundamental interaction for strong forces, i.e. QCD is also given. The concept of the effective mass of nucleon in the mean field created by mesons and their entropy distribution is duly addressed.

Chapter 3: − The equation of state (EoS) at zero temperature using the parameter sets FSUGarnet, IOPB-I, G3 along with the NL3 sets is examined in this chapter. The results reproduced are thoroughly compared with the available literature. Various properties of nuclear matter such as are saturation density, binding energy, incompressibility and effective mass etc. are investigated. The EoS is discussed in terms of incompressibility and meson couplings. The versatility of the used parameter set is studied and is

compared with the experimental data derived from various experiments. It is observed that the parameter sets FSUGarnet, IOPB-I and G3 have an extensive range of operation and can be used for describing nuclear matter at both normal and supernormal density. The scalar and vector potential are discussed in view of relativistic calculations.

Chapter 4: − The calculation of liquid-gas phase transition for the nuclear matter is presented for the first time using the E-RMF sets FSUGarnet, IOPB-I, G3 and the results are compared with NL3 force parameter and relevant experiments. The phase transition is investigated for both symmetric and asymmetric nuclear matter. The EoS, effective mass and entropy are also calculated and results are discussed in this chapter. For finite temperature limit, the suitability of used parameter sets and E-RMF formalism is discussed. The role of each meson in the E-RMF Lagrangian is investigated at finite temperature, and their corresponding effects are duly analysed. It is seen that all the RMF and E-RMF parameters including this work underestimate the critical temperature and pressure. One needs to find a higher order interaction term in the Lagrangian to account for this discrepancy. These parameter sets behave differently due to their different vector self-coupling terms which play a significant role in determining EoS at finite temperature.

5.2 Future Scope

The ultimate goal of the scientific community is to unravel the deepest secrets of the universe and more fundamentally to find how it all began. In that direction, several experiments like LIGO, VIRGO, RHIC, STAR, PHENIX, ALICE, CMS and ATLAS have made significant advancement in terms of gravitational wave detection to simulating Quark-Gluon Plasma. The Quark-Gluon Plasma is a consequence of core collapse supernova and one hope to witness it in our galaxy to know the inside of it. Meanwhile, it is customary to develop the theoretical understanding of this phenomenon, and this work finds the direct application on that front. The phase transition studied here can be extended to the QGP phase transition which is depicted in Fig. 1.1.

The EoS can also be calculated including baryon octet species at finite temperature, and subsequently, with the quark phase in the core, a complete picture of neutron star with a phase change in baryon to quark can be formulated at T=0 and finite temperature. This information will help to determine the properties of the stars at some finite temperature.

The present form of RMF can be modified to account for the deviation in theoretical predictions and experimental results in finite temperature case. For this, one needs to recalibrate the parameters to accommodate a higher order interaction term which may modify the results at finite temperature but keep the behaviour at zero temperature intact.

Bibliography

[1] J. Chadwick, *Nature* **129** (1932) 312 .

[2] E. Schrödinger, *Phys. Rev.* **28** (1926) 1049.

[3] M. Garçon and J. W. Van Orden, *Adv. Nucl. Phys.* **26** (2001) 293.

[4] Igal Talmi, *Nucl. Phys. A* **507** (1990) 295.

[5] I Mähr, F. Zappa, S. Denifl and D. Kubala et al., *Phys. Rev. Lett.* **98** (2007) 023401.

[6] B. P. Abbott et al., *Phys. Rev. Lett.* **119** (2017) 161101.

[7] Kazunori Akiyama et al., *ApJ* **875** (2019) L1 17pp.

[8] Walter C. Ermler et al., *Adv. Quantum chem.* **19** (1988) 139.

[9] R. P. Feynman, *Phys. Rev.* **76** (1949) 769.

[10] Steven Weinberg, *arXiv* [**hep-th**] (1996) 9702027 .

[11] Michael W. Kirson, *Nucl. Phys. A* **798** (2008) 29.

[12] Laurie M. Brown, *Physics Today* **39** (1986) 12.

[13] J.D. Walecka. *Theoretical Nuclear and Subnuclear Physics*. Imperial College Press, 2004.

[14] B. D. Serot and J. D. Walecka. *Advances in Nuclear Physics*. Plenum Press, New York, (1986).

[15] A. Hewis et al., *Nature* **217** (1968) 709.

[16] J. R. Oppenheimer and G. M. Volkoff, *Phys. Rev.* **55** (1939) 374.

[17] Luciano Rezzolla, Elias R. Most and Lukas R. Weih, *ApJ* **852** (2018) L25.

[18] Hans-Thomas Janka, *Annu. Rev. Nucl. Part. S.* **62** (2012) 407.

[19] C Markakis et al., *J. Phys.: Conf. Ser.* **189** (2009) 012024.

[20] Doan Thi Loan, Ngo Hai Tan, Dao T. Khoa, and Jerome Margueron, *Phys. Rev. C* **83** (2011) 065809.

[21] B.L. Berman and S.C. Fultz, *Rev. Mod. Phys.* **47** (1975) 713.

[22] G. Colo, U. Garg and H. Sagawa, *Eur. Phys. J. A* **50** (2014) 26.

[23] R. N. Panda, M. Panigrahi, Mahesh K. Sharma, and S. K. Patra, *Phys. Atom. Nuclei* **81** (2018) 417.

[24] Tuhin Malik, N. Alam, M. Fortin and C. Providência et al., *Phys. Rev. C* **98** (2018) 035804.

[25] L. I. Schiff, *Phys. Rev.* **84** (1951) 1.

[26] M. H. Johnson and E. Teller, *Phys. Rev.* **98** (1956) 783.

[27] H. P. Düerr and E. Teller, *Phys. Rev.* **101** (1956) 494.

[28] P. G. Reinhard, *Rep. Prog. Phys.* **52** (1989) 439.

[29] G. A. Lalazissis, J. König and P. Ring, *Phys. Rev. C* **55** (1997) 540.

[30] Abdul Quddus, K. C. Naik and S K Patra, *J. Phys. G: Nucl. Part. Phys.* **45** (2018) 075102.

[31] S. Gmuca, *Nucl. Phys. A* **547**, (1992) 447; J. K. Bunta and S.Gmuca, *Phys. Rev. C* **68** (2003) 054318 .

[32] Todd-Rutel B G and Piekarewicz J *Phys. Rev. Lett.* **95** (2005) 122501; Horowitz C J and Piekarewicz J *Phys. Rev. Lett.* **86** (2001) 5647.

[33] R. J. Furnstahl, B. D. Serot and H. B. Tang, *Nucl. Phys. A* **615** (1997) 441.

[34] Abdul Quddus, M. Bhuyan, Shakeb Ahmad, B. V. Carlson, and S. K Patra, *Phys. Rev. C* **99** (2019) 044314.

[35] P. Arumugam, B. K. Sharma, P. K. Sahu, S. K. Patra, T. Sil, M. Centelles and X. Viñas, *Phys. Lett. B* **601** (2004) 51.

[36] Y. K. Gambhir, and A. Bhagwat, *Phys. Part. Nuclei* **37** (2006) 194.

[37] L. S. Kisslinger, *Phys. Rev.* **733** (1956) 1077.

[38] H. Müller and B. D. Serot, *Phys. Rev. C* **52** (1995) 2072.

[39] P. Wang, *Phys. Rev. C* **61** (2000) 054904.

[40] M. Mahi et al., *Phys. Rev. Lett.* **60** (1988) 1936.

[41] J. E. Finn et al., *Phys. Rev. Lett.* **49** (1982) 1321.

[42] J. Pochodzalla et al., *Phys. Rev. Lett.* **75** (1995) 1040.

[43] M. L. Gilkes et al., *Phys. Rev. Lett.* **73** (1994) 1590.

[44] S. S. Avancini, S. Chiacchiera, D. P. Menezes and C. Providencia, *Phys. Rev. C* **85** (2012) 059904.

[45] P. Bonche and D. Vautherin, *Nucl. Phys. A* **372** (1981) 496; Li Zeng-Hua, Zuo Wei and Lu Guang- Cheng, *Chinese Phys. Lett.* **21** (2004) 29.

[46] J. Heyer, T. T. S. Kuo, J. P. Shen and S. S. Wu, *Phys. Letts. B* **202** (1988) 465.

[47] P. K. Sahu, T. K. Jha, K. C. Panda and S. K. Patra, *Nucl. Phys. A* **733** (2004) 169.

[48] M. Malheiro, A. Delfino and C. T. Coelho, *Phys. Rev. C* **58** (1998) 426; Guo Hua, Liu Bo and M. Di Toro, *Phys. Rev. C* **62** (2000) 035203.

[49] L. McLerran, *Nucl. Phys. Proc. Suppl.* **195** (2009) 275.

[50] Bharat Kumar, S. K. Patra and B. K. Agrawal, *Phys. Rev. C* **97** (2018) 045806.

[51] H. Müller and B. D. Sero, *Nucl. Phys. A* **606** (1996) 508 .

[52] Del Estal M, Centelles, X. Viñas and S. K. Patra, *Phys. Rev. C* **63** (2001) 024314.

[53] P. Ring, *Prog. Part. Nucl. Phys.* **37** (1996) 193.

[54] R. J. Furnstahl, C. E. Price, and G. E. Walker, *Phys. Rev. C* **36**, (1987) 2590 .

[55] J. D. Walecka, *Ann. Phys.* **83** (1974) 491.

[56] Ch. C. Moustakidis and C. P. Panos, *Phys. Rev. C* **79** (2009) 045806.

[57] W. C. Chen and J. Piekarewicz, *Phys. Lett. B* **748**, (2015) 284.

[58] Bharat Kumar, S. K. Singh, B. K. Agrawal and S. K. Patra, *Nucl. Phys. A* **966** (2017) 197.

[59] Pieper S C, Pandharipande V R, Wiringa R B and Carlson J., *Phys. Rev. C* **64** (2001) 014001.

[60] K. Hebeler, J. M. Lattimer, C. J. Pethick, and A. Schwenk, *Astrophys. J.* **773** (2013) 11.

[61] B. Friedman and V. R. Pandharipande, *Nucl. Phys. A* **361** (1981) 502.

[62] B. K. Sharma, P. K. Panda, and S. K. Patra, *Phys. Rev. C* **75** (2007) 035808.

[63] Bharat Kumar and S. K. Biswal, and S. K. Patra, *Phys. Rev. C* **95**, (2017) 015801.

[64] K Nakamura and Particle Data Group 2010 J. *Phys. G: Nucl. Part. Phys.* **37** (2017) 075021.

[65] Bharat Kumar, S. K. Biswal and S. K. Patra, *Phys. Rev. C* **95** (2017) 015801.

[66] P. Danielewicz, R. Lacey and W. G. Lynch, *Science* **298** (2002) 1592.

[67] A. W. Steiner, J. M. Lattimer and E. F. Brown, *Astrophys. J.* **722** (2010) 33.

[68] J. Nättilä, A. W. Steiner, J. J. E. Kajava, V. F. Suleimanov and J. Poutanen *Astron. Astrophys.* **591** (2016) A25.

[69] T. Li et al., *Phys. Rev. C* **49** (1994) 1630.

[70] J. B. Elliott, P. T. Lake, L. G. Moretto and L. Phair, *Phys. Rev. C* **87** (2013) 054622.

[71] J. B. Silva, O. Lourenço, A. Delfino, J. S. Sá Martins and M. Dutra, *Phys. Lett. B* **664** (2008) 246.

[72] N. Alam, H. Pais, C. Providencia and B. K. Agrawal, *Phys. Rev. C* **95** (2017) 055808.

Vishal Parmar_MSc_Thesis_V2

ORIGINALITY REPORT

Sub. I-D. → 112043872 8

7%	2%	7%	1%
SIMILARITY INDEX	INTERNET SOURCES	PUBLICATIONS	STUDENT PAPERS

PRIMARY SOURCES

1	Abdul Quddus, Kishor Chandra Naik, S K Patra. "Study of hot thermally fissile nuclei using relativistic mean field theory", Journal of Physics G: Nuclear and Particle Physics, 2018 Publication	1%
2	Abdul Quddus, M. Bhuyan, Shakeb Ahmad, B. V. Carlson, S. K. Patra. "Temperature-dependent symmetry energy of neutron-rich thermally fissile nuclei", Physical Review C, 2019 Publication	1%
3	Bharat Kumar, S. K. Patra, B. K. Agrawal. "New relativistic effective interaction for finite nuclei, infinite nuclear matter, and neutron stars", Physical Review C, 2018 Publication	1%
4	Sahu, P.K.. "Hot nuclear matter in asymmetry chiral sigma model", Nuclear Physics, Section A, 20040308 Publication	<1%

4/5/2020